University of California
Los Angeles

Correlations with Non-Photonic Electrons in $\sqrt{s_{NN}} = 200$ GeV AuAu Collisions in STAR

A dissertation submitted in partial satisfaction
of the requirements for the degree
Doctor of Philosophy in Physics

by

Lloyd Edward Dunkelberger Jr.

2015

The dissertation of Lloyd Edward Dunkelberger Jr. is approved.

University of California, Los Angeles

2015

Table of Contents

List of Figures

List of Tables

CHAPTER 1

Introduction

CHAPTER 2

Experimental Setup

2.1 Relativistic Heavy Ion Collider

2.2 STAR Detector

2.3 Time Projection Chamber

2.4 Barrel Electromagnetic Calorimeter

CHAPTER 3

Identification of Non-photonic Electrons

We discuss the procedure for identifying electrons in events at STAR and how we remove photonic background. We show the event and track selection criteria and then lastly we will analyze the efficiency for identifying background photonic electrons. The identification of non-photonic electrons (NPE) and efficiency thereof will be critical factors when we construct the NPE-hadron correlations in later chapters.

3.1 Outline of the NPE Identification

This chapter will lay out the general methods for event selection, track selection, electron identification, and the removal of photonic electron background for both Au+Au and p+p collisions.

We start by identifying the dataset and the trigger collections we will use for the analysis. We look at the events and check that the quality of the event is good and that there could be candidate tracks for NPE in the event. We then reconstruct all tracks in the TPC and apply track quality cuts. To identify electrons we rely on the energy loss (dE/dx) measured in the TPC and on the hits in the EMC towers and shower max detector.

The background from photonic electrons will be removed by searching for the opposite signed partner electron. If the primary track is from Dalitz decays or photon conversion in the detector, the partner and primary track should have a low invariant mass. We will also investigate, through simulations, the efficiency for determining the background from photonic electrons.

In the end we will have a sample of electrons which we can use as triggers for measuring

NPE-hadron correlations.

3.2 Dataset and Event Selection

3.2.1 Data and Triggers

In 2011 RHIC collided gold nuclei at $\sqrt{s_{NN}} = 200$ GeV and delivered 9.79 nb^{-1} integrated luminosity similar to what was delivered during the previous year's run. The STAR detector recorded about 1.1 billion events across all triggers with TPC and BEMC information. In 2012 polarized proton collisions were run in RHIC (the polarization of the beams is not relevant to this analysis) at the same 200 GeV beam energy. RHIC delivered 74.0 pb^{-1} which resulted in 1.7 billion triggered events in STAR. Heavy flavor events are rare and detector efficiencies can be low meaning the NPE analysisis typically constrained by statistics, necessitating large data sets. The Silicon Vertex Tracker (SVT) was removed from STAR resulting in less material near the beam line which cuts down on background from conversions in the detector. This combination of low material and high statisics make runs 11 and 12 (prior to run 14) the best datasets available for the analysis of non-photonic electrons.

The STAR data acquisition system handles several different triggers the most commonly used is the minimum bias trigger (minbias) which fires based on the coincidence of the STAR vertex position detector(VPD) and Zero Degree Calorimeters (ZDC) these events are prescaled so that only a fixed fraction of triggers are accepted so that the DAQ's data taking rate is not exceeded. STAR can also trigger on hits in the barrel EMC, these are the high tower (HT) triggers. A high tower trigger requires that a hit in a BEMC tower exceeds an ADC threshold determined such that the transverse energy in that tower is high. In run 11 we use the HT triggers NPE11, NPE15, NPE18, and NPE25 which are in increasing order of E_T. The NPE11 and NPE15 triggers are also prescaled. In p+p we use the BHT0, BHT1, BHT2, and BHT3 triggers, of these only BHT0 is prescaled.

Due to the large dataset sizes it is in our best interest to cut down on the data we need

whenever possible. We do this first when we read the data to make BEMC points to match to tracks. Here we look through the tracks in the event and search for electron candidates based on the TPC information only. We throw out events without viable electron candidates. Since these cuts are looser than the electron cuts we will apply later we don't remove events we might actually want and we retain the ability to tighten the cuts later if we need to. After limiting ourselves to high tower triggers and keeping only events with electron candidates we are left with approximately 23 million events in Au+Au and 1.1 million events in p+p.

3.2.2 Event Level Cuts

3.3 Track Reconstruction and TPC Cuts

3.4 BEMC Points and Matching

3.5 Electron Purity

3.6 Photonic Electron Identification

3.7 Photonic Electron Reconstruction Efficiency

CHAPTER 4

Azimuthal Correlations of Non-Photonic Electrons to Hadrons

We will now investigate the correlations of triggered non-photonic electrons to hadrons in $Au + Au$ and $p + p$ collisions at 200 GeV. Hard processes in these collisions will produce back to back jets in the azimuthal angle ϕ. We search for potential modification of the jet in $Au + Au$ collisions compared to $p + p$.

4.1 Overview of Constructing the NPE-hadron Correlation

Several steps are needed to produce the NPE-h correlation. The trigger particle electrons are identified by the procedure described in the previous chapter. The nonuniform acceptance of detector results in false correlations which are not a result of the underlying physics. This is corrected in two ways, the ϕ distribution of all particles in flattened and then the correlations from mixed events are calculated and then a weighting is determined so as to flatten these as well.

In correlations from $Au+Au$ collisions there is an underlying background correlation from the flow of the both the trigger electron and the associated hadron. In this analysis we only consider the second order harmonic of flow, v_2. For hadrons, v_2 is very accurately measured across a wide range centralities and p_T. For non-photonic electrons, the measurements of v_2 are not so precise, thus we can only estimate its contribution to the background. This uncertainty will be reflected in the analysis of systematic error.

We will also look at the dependence of the correlation on the angle between the trig-

gered electron and the event plane. A dependence on this angle could point to path length dependence on the jet suppression in QGP.

4.2 Acceptance Corrections

The STAR detector give full 2π azimuthal coverage, however there are still regions of the detector which have noticeably poorer efficiency. This causes an uneven azimuthal acceptance which in turn lead to spurious correlations between detected particles. To correct this we need to apply a weighting to each track depending on where it is in the detector.

4.2.1 Single Particle ϕ-weighting

We begin by correcting for the single particle acceptance in ϕ. The boundaries between sectors produce regions of lower efficiency, also in Run11 one sector of the TPC had noticeably lower efficiency than the rest. These effects are both shown in Figure 4.1.

The dependence of the acceptance on ϕ however is not the same for all tracks. Whether a track crosses a sector boundary or passes through the dead sector will depend on that particular track's geometry. Tracks at low p_T curve more in the magnetic field and thus the effects of these lower efficiency areas apply to wider regions in track ϕ. The dependence of acceptance on p_T is shown in Figure 4.2. At low p_T the dependence is especially strong thus for $p_T \leq 1$ GeV/c we divide tracks into p_T bins of .1 GeV/c, which is near the limit of the momentum resolution of the TPC. Above 1 GeV/c the tracks are roughly straight so the effects on acceptance from the sector boundaries and dead sector are consistent bin-to-bin up to arbitrarily large p_T.

While the dependence of acceptance on track p_T is by far the largest effect, we still further subdivide the tracks to make acceptance corrections. It is possible for the acceptance to depend on η, and we are especially concerned with edge effects when $|\eta| \sim 1$, thus we divide into 4 even bins in pseudorapidity ranging from -1 to 1.

Likewise we account for dependence on the event vertex (in both $p + p$ and $Au + Au$)

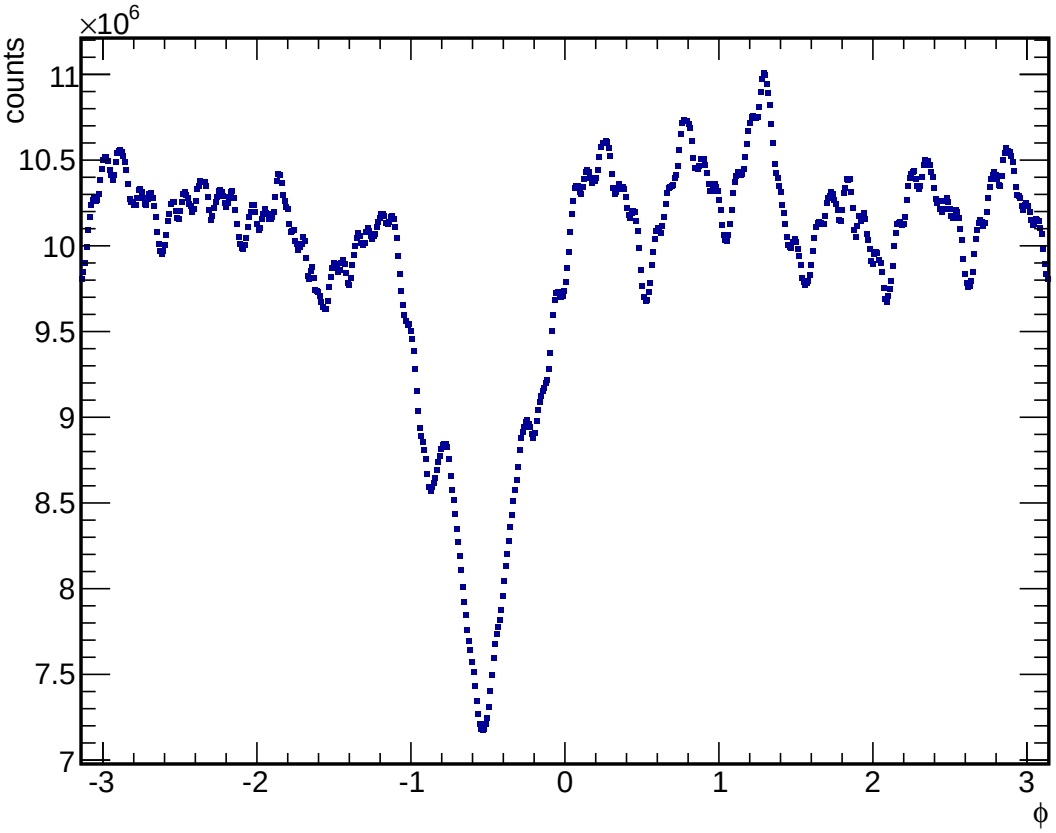

Figure 4.1: The azimuthal angular distribution of all tracks in Run11 $Au + Au$ collisions at 200 GeV. Periodic bumps can be seen from the sector boundaries, as well as a dip in the poorly performing sector.

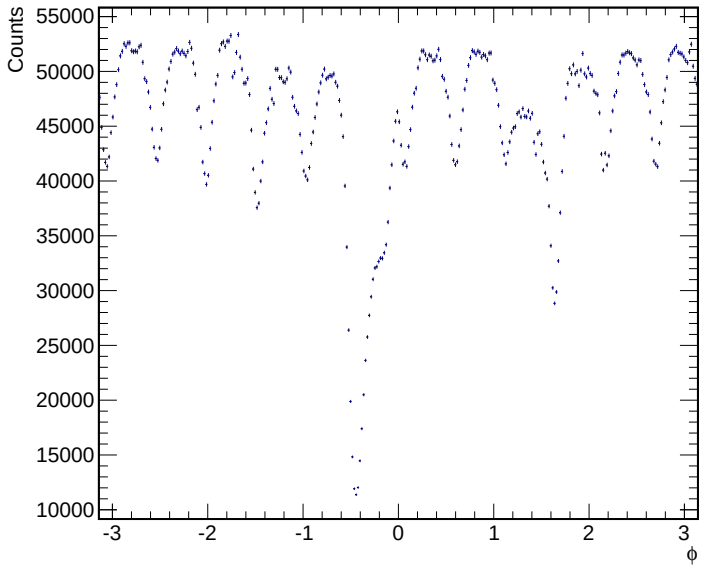

(a) .5 GeV/c $\leq p_T \leq$ 1.0 GeV/c

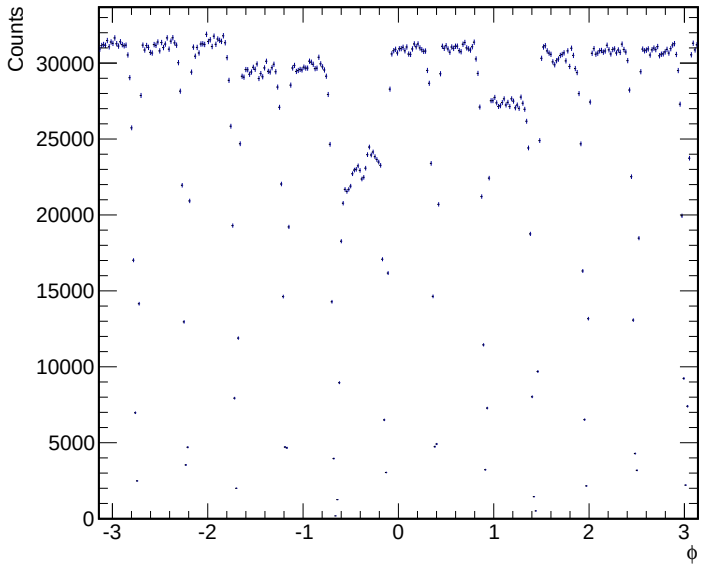

(b) 1.5 GeV/c $\leq p_T \leq$ 2.0 GeV/c

Figure 4.2: ϕ distributions for single particles in different p_T bins. Strong p_T dependence is seen especially below 1 GeV/c due to the different track geometries.

and multiplicity (only for $Au + Au$) by dividing into bins of vertex-z and centrality. For the centrality bin divisions, all centrality bins from $30\% - 80\%$ are taken together since in the peripheral bins the statistics are too low to get a reliable acceptance correction.

Finally, since the tracks in the TPC are curved, there will be a dependence on which direction the track curves. For example, two particles may start on opposite sides of a sector boundary separated by some distance in ϕ but both may cross the boundary if they curve in opposite directions. So we need to take separate weightings based on the product of the magnetic field and the particle's charge, $B \cdot q$.

After calculating the single ϕ correction we apply it to each track in the analysis whenever we calculate event planes or 2-particle correlations. Since some areas of the detector have very low efficiencies they can introduce huge weights for a small number of particles. This can destabilize results, so we cap the weight an individual particle can get at 5.0.

4.2.2 Mixed Event Background

To further correct for nonuniformities is detector acceptance we use a mixed event weighting. In an ideal detector the correlations of trigger particles to associated hadrons from a different event should be flat, however acceptance effects will result in nonphysical correlations which need to be removed.

Similar to the single particle corrections we divide the mixed event corrections into bins to account for various systematic differences. In mixed event we bin according to associated particle p_T, triggered particle p_T, centrality, vertex z position, and η. As in single particle corrections, the most extreme bin to bin variationsoccur between the low associated p_T bins.

4.3 Background from Flow

4.3.1 Measurements of Flow

The motivations behind two-particle correlation studies are typically the investigation of jet modification in QGP and the response of the medium to jets. But even in the absence of jets

we still expect to see some correlation within events from flow. The azimuthal anisotropy resulting from the second order flow harmonic, v_2, of both the trigger and associated particles produces a background shape with the form:

$$B[1 + v_2^{trig} v_2^{asso} \cos(2\Delta\phi)] \tag{4.1}$$

where B is an overall constant factor. Higher order harmonics v_3, v_4, etc. can also contribute to the background. Large v_3 in particular is a potential explanation for some of the results in dihadron correlations, but these effects are not considered for this analysis.

Hadron v_2 has been measured to high precision in a wide range of p_T bins at STAR. Figure 4.3 shows the results of STAR v_2 measurements using an event plane method and illustrates the general depedence on p_T and centrality. To calculate the hadron v_2 we extrapolate the v_2 measurement to the center of the associated hadron p_T bin. Then when looking at correlations across multiple hadron p_T bins we use the weighted average of v_2 based on the number of hadrons in each p_T bin.

Measurements of electron v_2 at STAR have shown that non-photonic electrons also have large elliptic flow. Because of limited statistics electron v_2 is measured in much larger p_T and centrality bins. Various measurements of NPE v_2 are seen in Figure 4.4, showing that they tend to fall in a range between .05 and .15 depending on the measurement procedure. For this analysis we assume that NPE v_2 is .1 in all bins, we then vary the NPE v_2 between .05 and .15 and take the difference in final correlations as a systematic error.

4.3.2 Background Normalization

Knowing the values of v_2 for hadrons and non-photonic electrons, we then need to determine the overall normalization constant B as in Equation 4.1. There are two simple ways of estimating this, both relying on the assumption that the jet like contributions to the azimuthal correlation are concentrated in peaks around 0 and π, and that any remaining correlations there are the result of the underlying v_2 background.

In one case we can simply pick a point between the near and away sides and then set B so

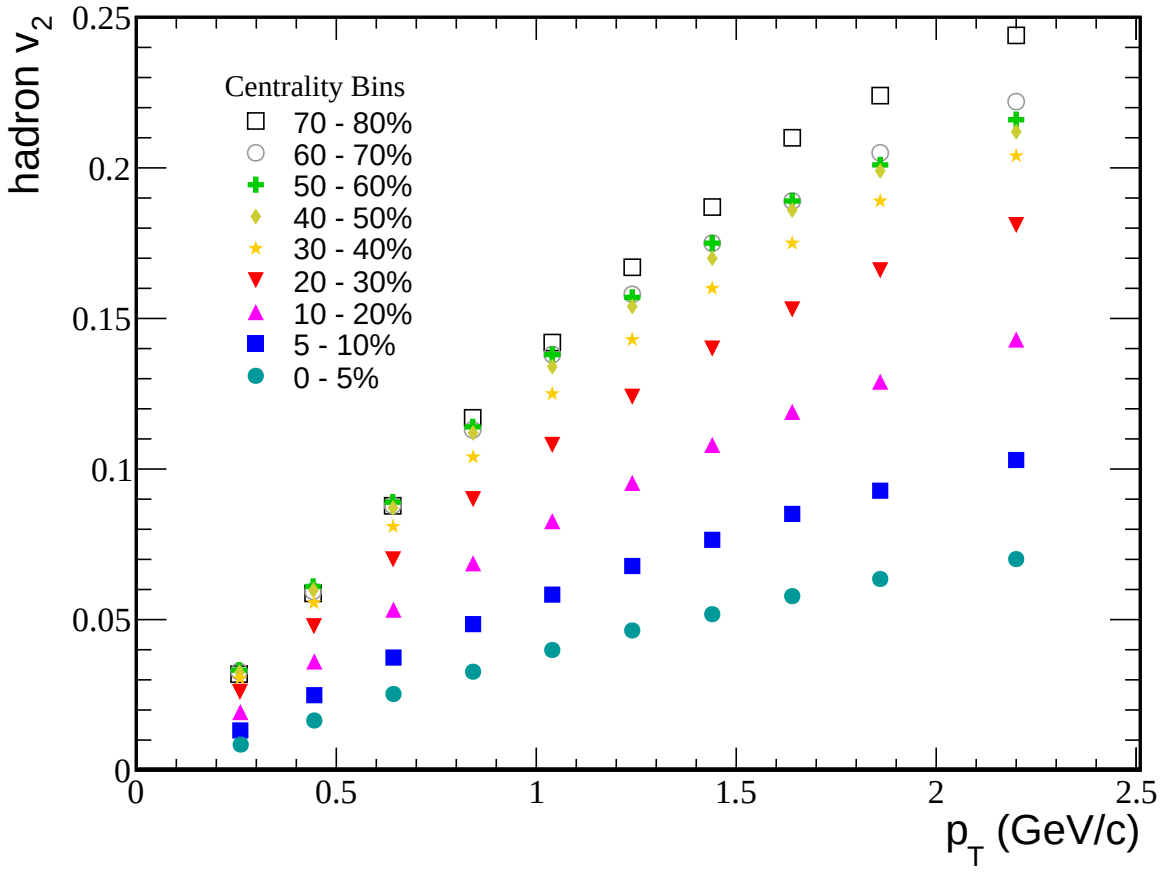

Figure 4.3: Measured v_2 values for hadrons across a range of p_T and centralities.

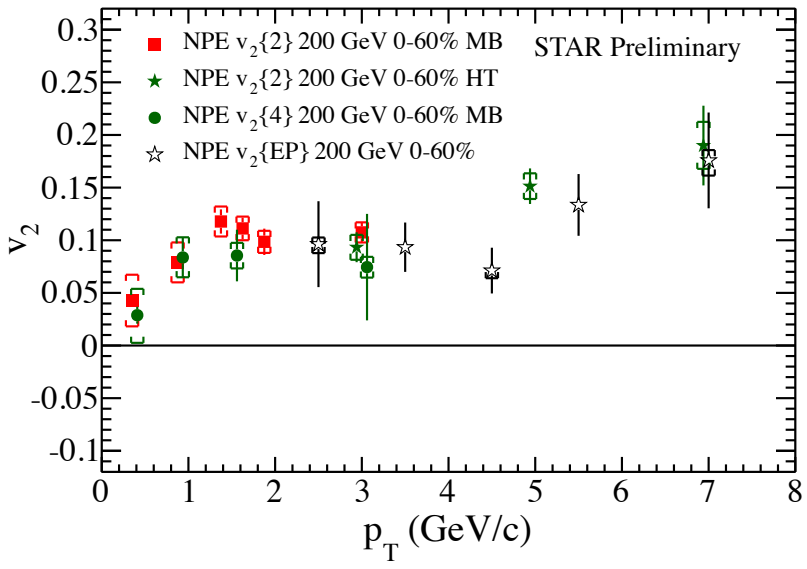

Figure 4.4: Various measurements of NPE v_2 in STAR. Going forward we assume .1 to be the value for NPE v_2 in all bins.

that the overall yield of particles above background at that point is 0. This point is typically taken to be around 1 radian and thus this method is called the zero yield at 1 (ZYA1) normalization. Although when we implent ZYA1 normalization we take the lowest absolute yield of the 3 points closest to 1 radian. Alternatively we can instead pick the point in the raw correlation with lowest value and normalize so that that point produces zero yield. This is the zero yield at minimum (ZYAM) method. These methods tend to coincide in practice and unless otherwise noted we use ZYAM normalization. There is another technique called absolute background subtraction used by PHENIX in their NPE-hadron correlation measurement but we do not use this method.

When using ZYAM or ZYA1 normalization our background subtracted yield can be very suceptible to downward fluctuations of points causing an abnormally high yield. To account for this we also look at the effect of normalizing to the next highest point in the correlation. We then compare the values of B that we get and then quote the difference as the systematic error of background normalization.

Variable	Cut
Track Type	$< .5$ (Primary)
Global DCA	< 2.0cm
η	$\in (-1.0, 1.0)$
p_T	$\geq .2$ GeV

Table 4.1: Cuts for associated hadrons used in e-h correlations

4.4 Correlations in Au+Au

We will now look at putting together the results of the previous sections and creating the NPE-h correlation in Au+Au collisions. We will then discuss the results in Au+Au before moving on to p+p and event plane dependent correlations.

4.4.1 Associated Hadrons

The basic quantity we will measure is the yield $\frac{dN}{d\Delta\phi}$ of associated hadrons at various relative to some triggered electron. For the associated hadrons the cuts we use are summarized in Table 4.1.

The correlations are further broken up into bins in event centrality and associated hadron p_T. This is the point at which we apply the acceptance corrections from the single particle ϕ weighting as well as the mixed event weighting. Additionaly we also correct the yield for the efficiency of the associated hadron yield. The TPC efficiency is lower for the high occupancy events in central collisions, and efficiency is also significantly worse for very low p_T hadrons. The efficiency is calculated from embedding and the results are summarized in Figure 4.5.

4.4.2 Constructing the NPE-hadron correlation

Now with azimuthal electron-hadron correlation functions we look at how we create the NPE-h correlation. The definition of the NPE-h correlation is:

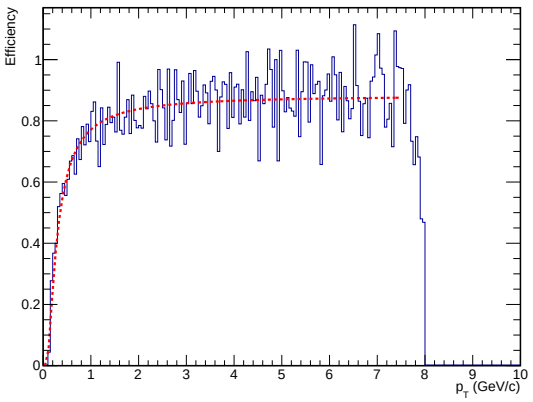

(a) 50-60%

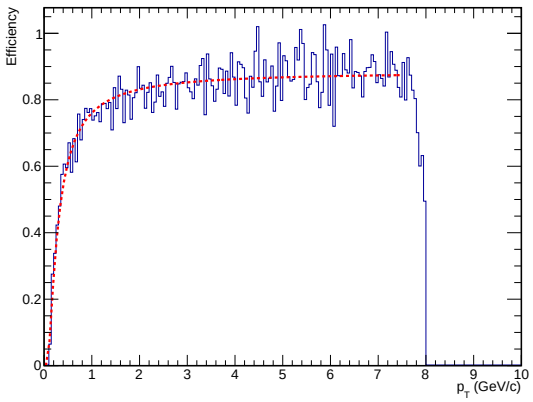

(b) 40-50%

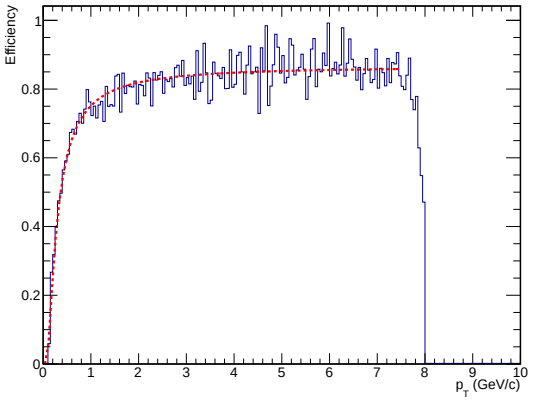

(c) 30-40%

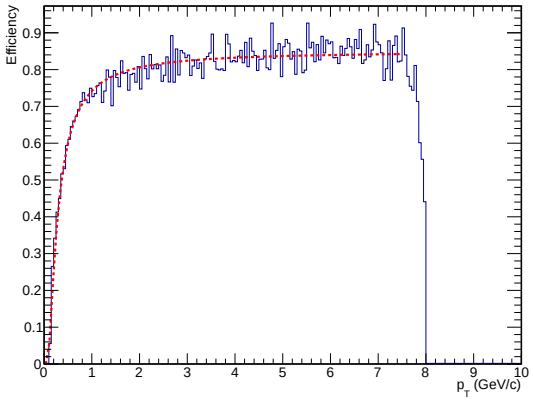

(d) 20-30%

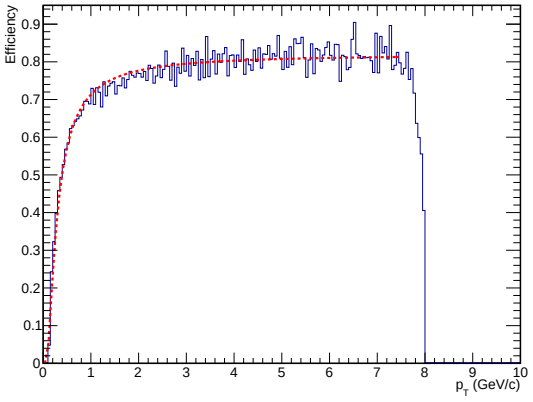

(e) 10-20%

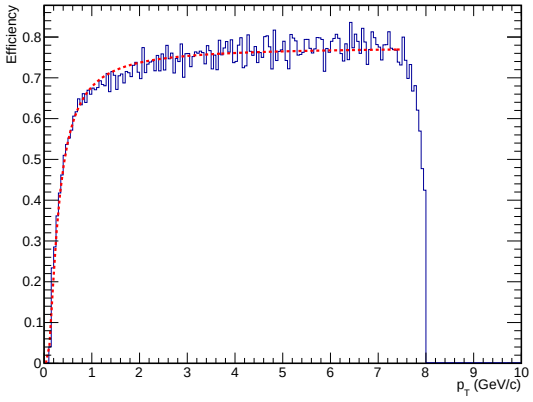

(f) 0-10%

Figure 4.5: The TPC efficiency for hadrons as a function of hadron p_T. The different plots are for different centralities which correspond to 0-10%, 10-20%, 20-30%, 30-40%, 40-50%, and 50-60%.

$$\frac{dN_{NPE-h}}{d\Delta\phi} = \frac{dN_{semi-h}}{d\Delta\phi} - \left(\frac{1}{\epsilon_\gamma} - 1\right)\frac{dN_{photonic-h}}{d\Delta\phi} + \frac{dN_{same-h}}{d\Delta\phi} \tag{4.2}$$

An explanation of these terms:

- **Semi-inclusive electrons:** This is the correlation of inclusive electrons for which no photonic partner track could be found. This sample will include many non-photonic electrons as well as some photonic background for which we could not find a partner track.

- **Unidentified photonic electrons:** the term:

  $$\left(\frac{1}{\epsilon_\gamma} - 1\right)\frac{dN_{photonic-h}}{d\Delta\phi}$$

  is intended to remove the remaining photonic background triggers from the semi-inclusive sample. To do this we take the correlation for identified photonic electrons to hadrons and scale it up according to the estimated photonic electrons reconstruction efficiency, ϵ_γ. The reconstruciton efficiency is determined by embedding simulations.

- **Same-sign electrons:** The method for identifying photonic electrons, pairing all tracks and calculating DCAs and invariant masses, will result in some oversubtraction of NPE signal. We account for the combinatorially removed points by looking at the results of same sign pairing tracks, i.e. the tracks which pass all of the photonic partner cuts except that they have the same sign. We add this term back make up for the NPE signal which was removed by the previous two terms.

There is also the potential for contamination of the triggered electrons with hadrons. This would require the subtraction of a dihadron correlation term:

$$\frac{dN_{h-h}}{d\Delta\phi}$$

We expect the purity of our triggered electrons to be high in the relevant p_T ranges so for this analysis we will not include it.

4.4.3 Raw Correlations

The raw correlation is the distribution $\frac{dN_{NPE-h}}{d\Delta\phi}$ before we subtract the background from v_2. The subtraction and correction spelled out in Equation 4.2 has already been performed and what is shown in the following figures is the NPE-h correlation with no background subtraction. The raw correlations serve as an initial check of the correlation method to spot any problems with our procedure.

Figures 4.6, 4.7and 4.8 show the raw correlations in 200 GeV AuAu collisions and that they conform to our rough expectations. Overall particle yields are also higher at lower p_T and are much higher in central events where multiplicity is higher. The general trend is for particle yields to be higher around 0 angle relative to the triggered NPE and at π, this is normal dijet distribution which is seen in hard processes. We also see that these dijets sit on top of a modulated background from v_2. We can see that the calculated backgrounds are reasonable and we also get a sense of the performance and limitations of the ZYAM method. For example in Figure 4.8a we see that a low fluctuation in one bin may have pulled down the normalization causing the near side peak to sit farther above the background. We will account for these types when we estimate the systematic uncertainties.

4.4.4 Subtracted Distributions and Yields

We now want to look at how the jet-like distributions of particles changes as a function of collision centrality and trigger particle p_T. We subtract off the background from the underlying event and v_2 to examine effects of the heavy quark fragmentation and propagation through the medium. The subtracted plots are summarized in Figures 4.9, 4.10and 4.11.

For these NPE-h correlations we also consider three sources of systematic error: Uncertainty from NPE v_2, uncertainty in photonic electron reconstruction efficiency, and background normalization. Results NPE v_2 are over wide ranges in p_T and centrality and are roughly around .1 we take that value when calculating the background but we also calculate backgrounds with v_2 of .05 and .15. We then take the difference between these extremes as the uncertainty.

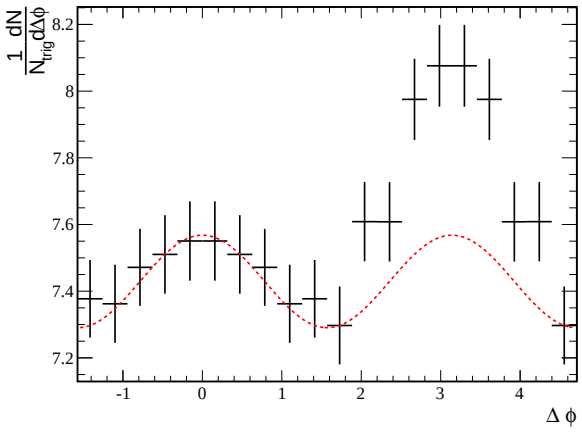

(a) .5 GeV/c $\leq p_{T,h} \leq$ 1.0 GeV/c

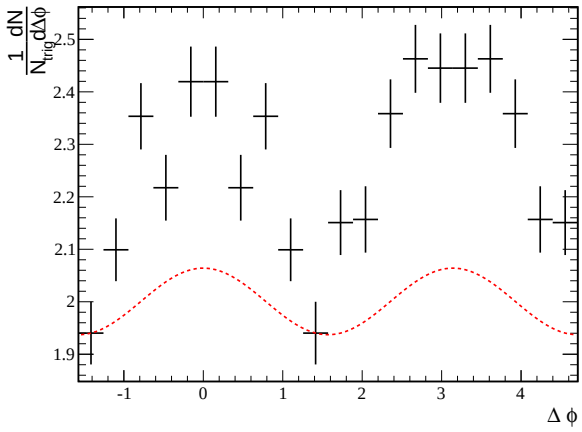

(b) 1.0 GeV/c $\leq p_{T,h} \leq$ 2.0 GeV/c

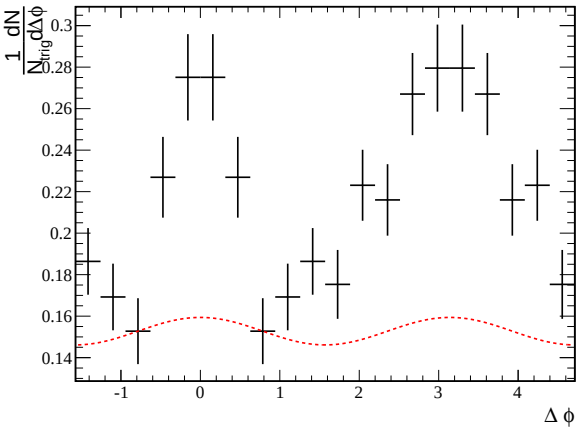

(c) 2.0 GeV/c $\leq p_{T,h} \leq$ 4.0 GeV/c

Figure 4.6: Raw NPE-h Correlations for 40-60% centrality events. Trigger p_T is 4.0 GeV/c $\leq p_{T,trig} \leq$ 6.0 GeV/c

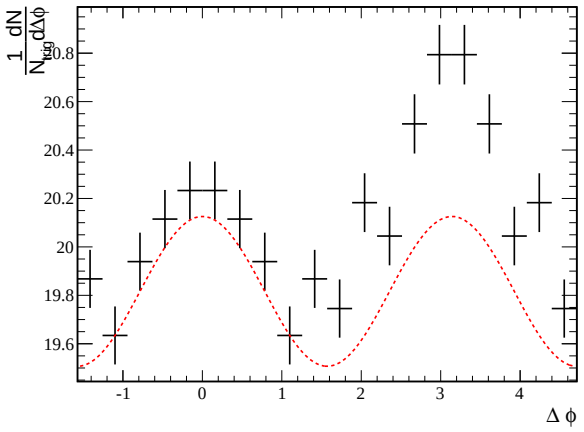

(a) .5 GeV/c $\leq p_{T,h} \leq$ 1.0 GeV/c

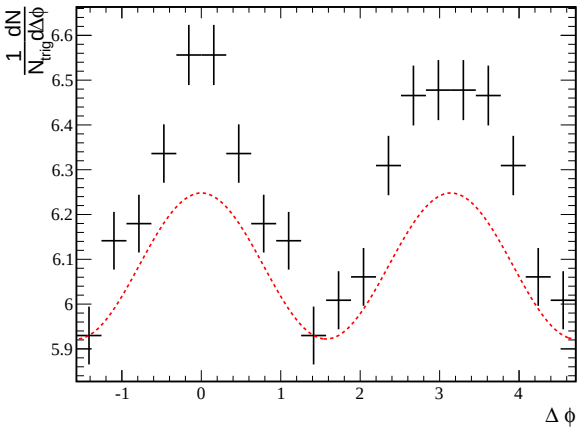

(b) 1.0 GeV/c $\leq p_{T,h} \leq$ 2.0 GeV/c

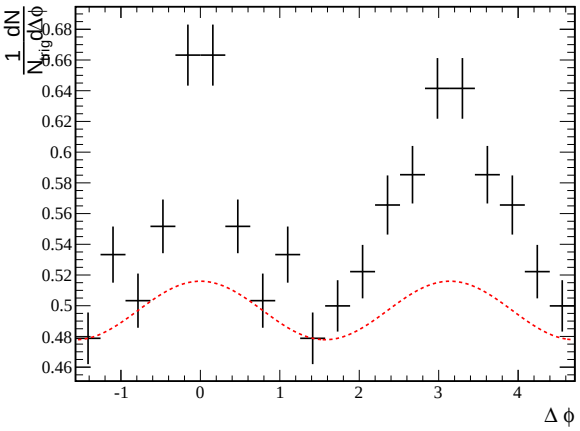

(c) 2.0 GeV/c $\leq p_{T,h} \leq$ 4.0 GeV/c

Figure 4.7: Raw NPE-h Correlations for 20-40% centrality events. Trigger p_T is 4.0 GeV/c $\leq p_{T,trig} \leq$ 6.0 GeV/c

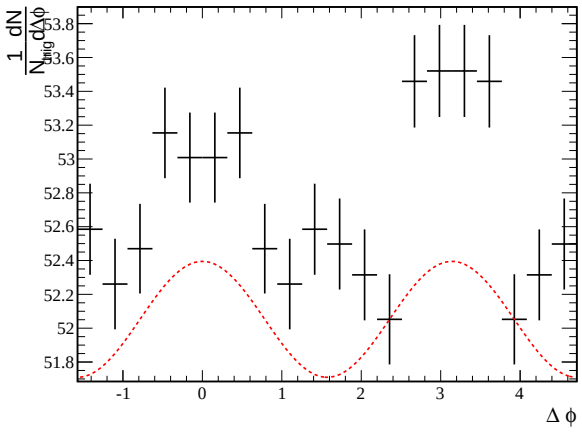

(a) .5 GeV/c $\leq p_{T,h} \leq$ 1.0 GeV/c

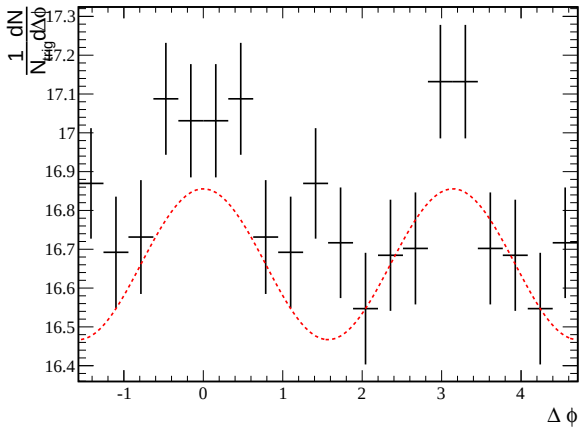

(b) 1.0 GeV/c $\leq p_{T,h} \leq$ 2.0 GeV/c

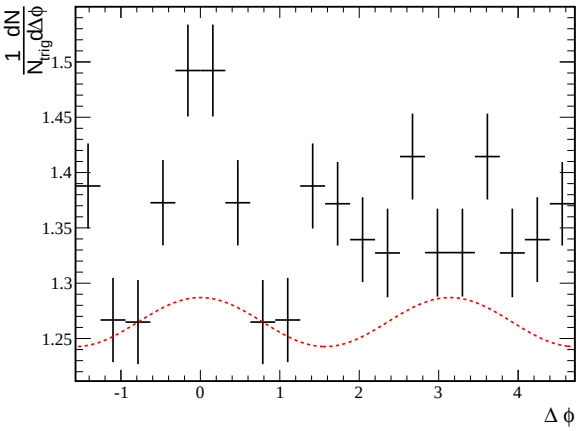

(c) 2.0 GeV/c $\leq p_{T,h} \leq$ 4.0 GeV/c

Figure 4.8: Raw NPE-h Correlations for 0-10% centrality events. Trigger p_T is 4.0 GeV/c $\leq p_{T,trig} \leq$ 6.0 GeV/c

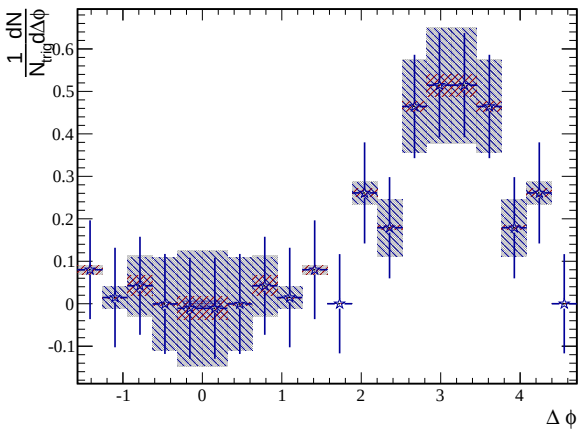

(a) .5 GeV/c $\leq p_{T,h} \leq$ 1.0 GeV/c

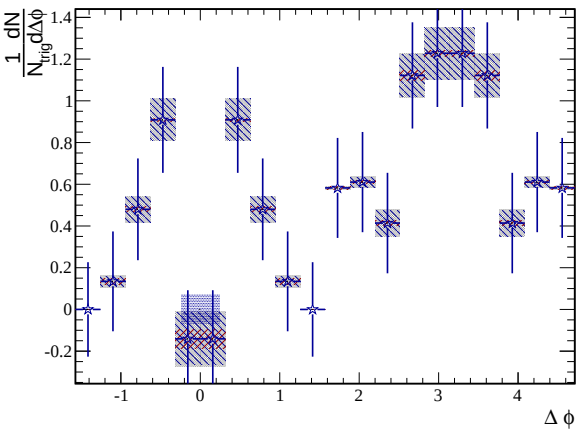

(b) .5 GeV/c $\leq p_{T,h} \leq$ 1.0 GeV/c

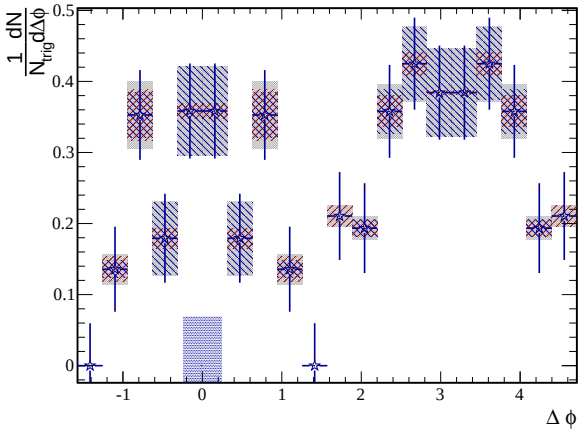

(c) 1.0 GeV/c $\leq p_{T,h} \leq$ 2.0 GeV/c

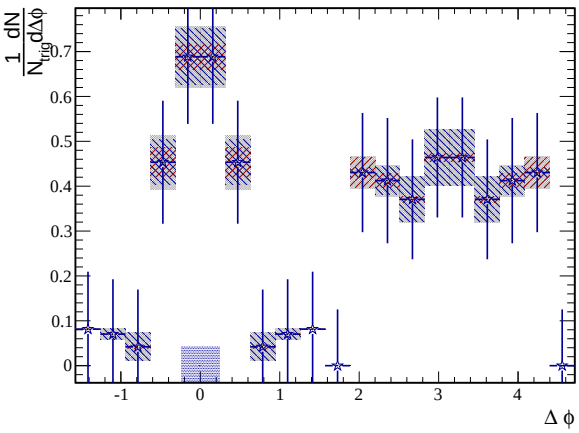

(d) 1.0 GeV/c $\leq p_{T,h} \leq$ 2.0 GeV/c

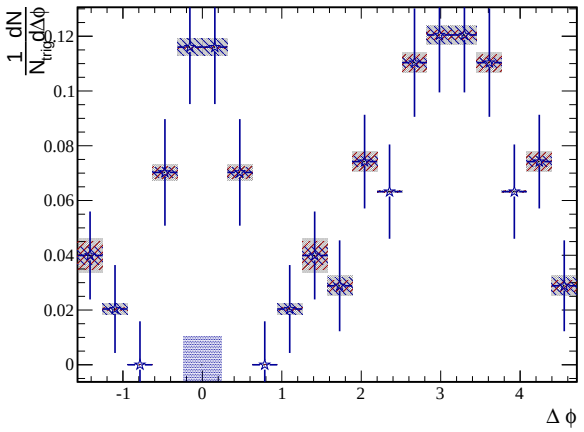

(e) 2.0 GeV/c $\leq p_{T,h} \leq$ 4.0 GeV/c

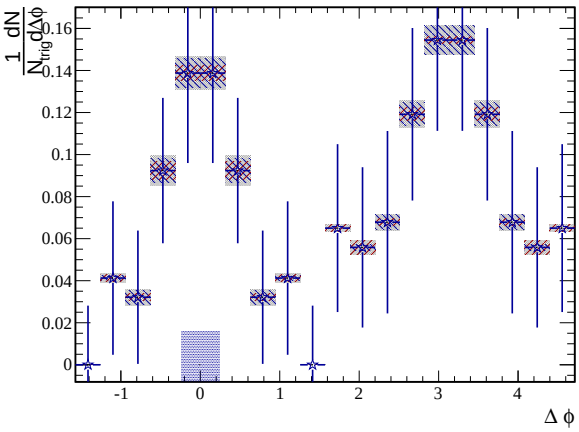

(f) 2.0 GeV/c $\leq p_{T,h} \leq$ 4.0 GeV/c

Figure 4.9: Background subtracted NPE-h correlations for 40-60% centrality events. Trigger p_T is 4.0 GeV/c $\leq p_{T,trig} \leq$ 6.0 GeV/c

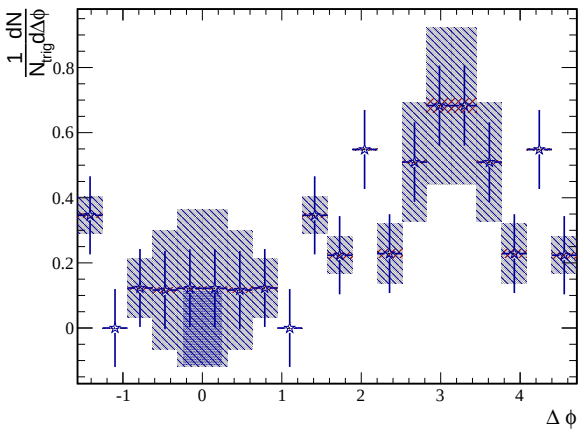

(a) .5 GeV/c $\leq p_{T,h} \leq$ 1.0 GeV/c

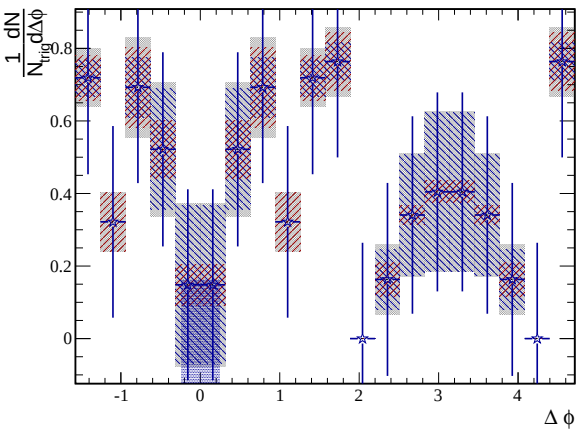

(b) .5 GeV/c $\leq p_{T,h} \leq$ 1.0 GeV/c

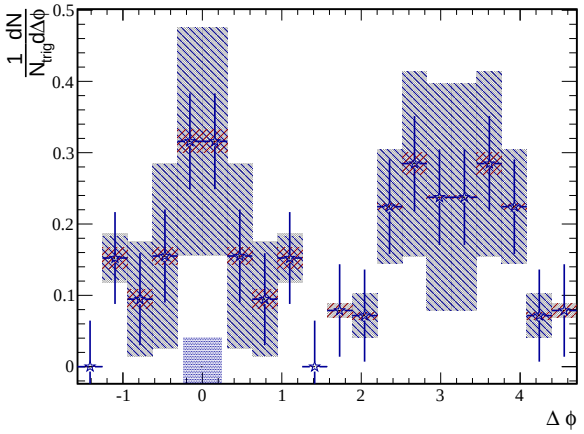

(c) 1.0 GeV/c $\leq p_{T,h} \leq$ 2.0 GeV/c

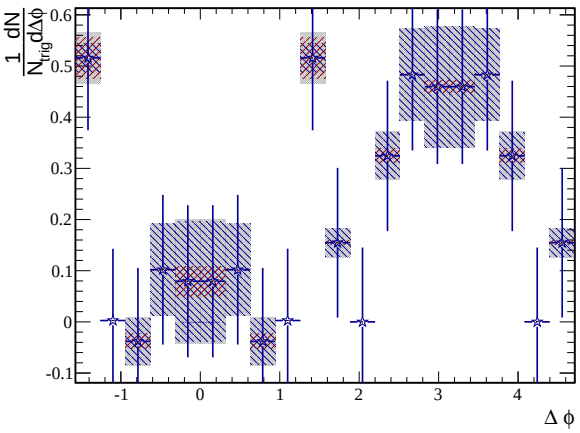

(d) 1.0 GeV/c $\leq p_{T,h} \leq$ 2.0 GeV/c

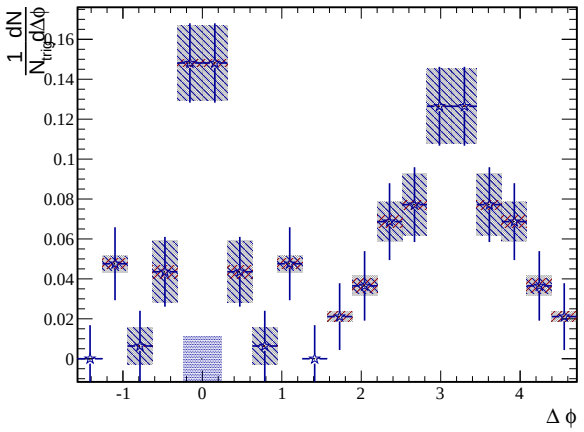

(e) 2.0 GeV/c $\leq p_{T,h} \leq$ 4.0 GeV/c

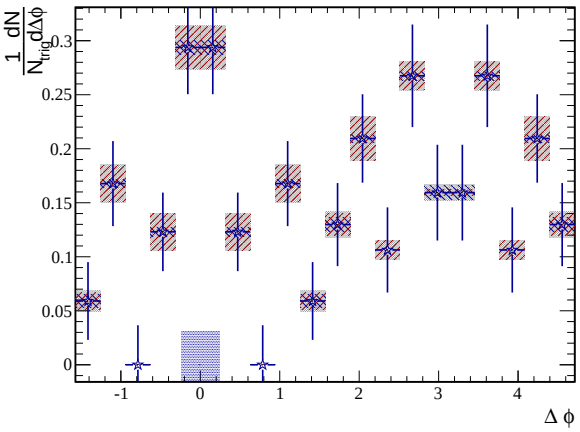

(f) 2.0 GeV/c $\leq p_{T,h} \leq$ 4.0 GeV/c

Figure 4.10: Background subtracted NPE-h correlations for 20-40% centrality events. Trigger p_T is 4.0 GeV/c $\leq p_{T,trig} \leq$ 6.0 GeV/c

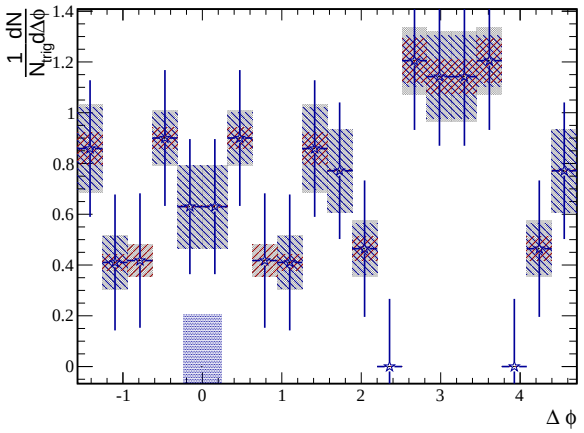

(a) .5 GeV/c $\leq p_{T,h} \leq$ 1.0 GeV/c

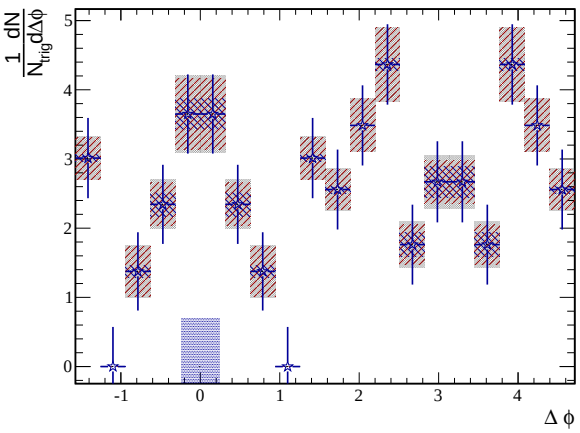

(b) .5 GeV/c $\leq p_{T,h} \leq$ 1.0 GeV/c

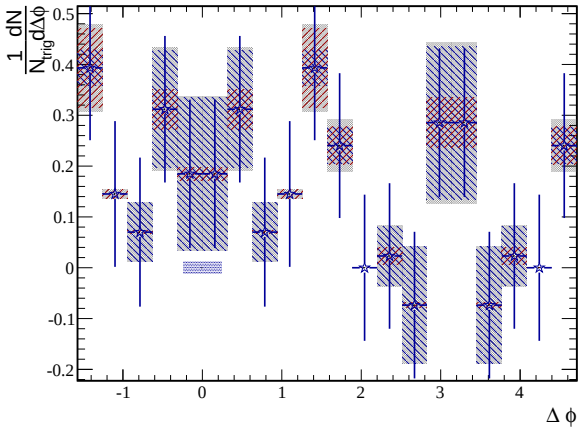

(c) 1.0 GeV/c $\leq p_{T,h} \leq$ 2.0 GeV/c

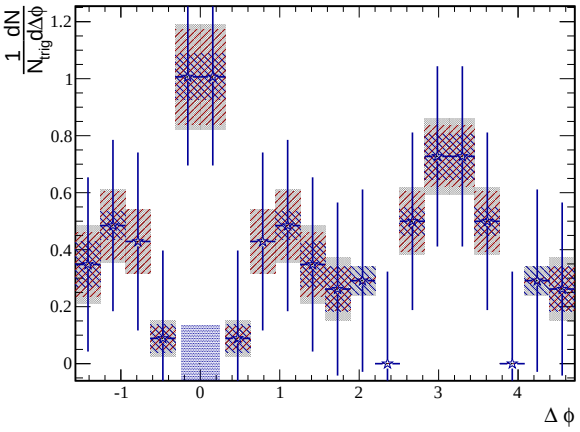

(d) 1.0 GeV/c $\leq p_{T,h} \leq$ 2.0 GeV/c

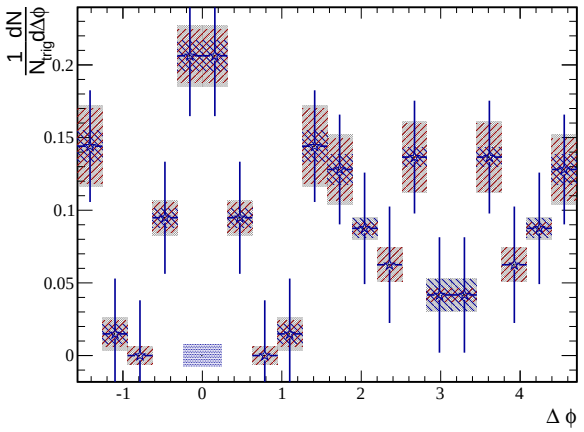

(e) 2.0 GeV/c $\leq p_{T,h} \leq$ 4.0 GeV/c

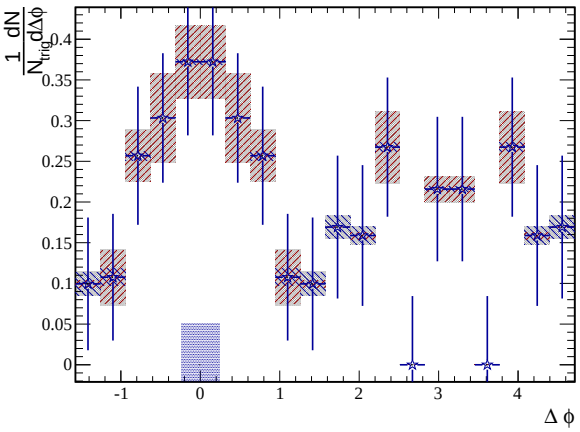

(f) 2.0 GeV/c $\leq p_{T,h} \leq$ 4.0 GeV/c

Figure 4.11: Background subtracted NPE-h correlations for 0-10% centrality events. Trigger p_T is 4.0 GeV/c $\leq p_{T,trig} \leq$ 6.0 GeV/c

Associated p_T	$\Delta\phi$ region	Yield $\frac{1}{N_{trigger}\Delta\phi}$	Stat. Error	Sys. Error
$p_{T,asso} \in (.5, 1.0)$ GeV/c	Near-side	0.0143632	0.0737196	0.0599507
$p_{T,asso} \in (.5, 1.0)$ GeV/c	Head	0.363855	0.0659528	0.0589941
$p_{T,asso} \in (.5, 1.0)$ GeV/c	Shoulder	0.107132	0.063884	0.00917141
$p_{T,asso} \in (1.0, 2.0)$ GeV/c	Near-side	0.322385	0.0396921	0.030521
$p_{T,asso} \in (1.0, 2.0)$ GeV/c	Head	0.366602	0.0355859	0.0283117
$p_{T,asso} \in (1.0, 2.0)$ GeV/c	Shoulder	0.126959	0.0335234	0.00708298
$p_{T,asso} \in (2.0, 4.0)$ GeV/c	Near-side	0.0649261	0.0114213	0.00148537
$p_{T,asso} \in (2.0, 4.0)$ GeV/c	Head	0.0923857	0.0105544	0.00160527
$p_{T,asso} \in (2.0, 4.0)$ GeV/c	Shoulder	0.0449183	0.00902871	0.00252461

Table 4.2: Yields and Errors from NPE-h correlations in 40-60% central Au+Au collisions with trigger 4.0GeV/c $\leq p_t \leq$ 6.0 GeV/c.

The photonic electron reconstruction efficiency (ϵ_γ) is determined from embedding simulations but the extracted values tend to vary from analysis to analysis. To be safe we allow the efficiency to vary by 10% and then take the difference in distributions as the error. This is done point by point. The combined NPE v_2 and ϵ_γ systematics are represented on the plots by the shaded region around the points. The NPE v_2 error tends to be the dominant source of uncertainty and the systematics are much larger for lower associated hadron p_T.

The systematic uncertainty from background normalization is calculated by performing the ZYAM procedure on the two lowest points in the correlation. The difference in normalization factors is taken as the uncertainty and we display this as a shaded bar at 0 yield and 0 angle. This uncertainty would move all points together in a uniform manner.

The subtracted distributions give some insight into the interactions of heavy quarks with the QGP medium. For all trigger p_T shown the direction of trigger electron is well correlated to the direction of the parent B or D meson. Thus we look to the near and away side yields for clues to the nature of the initially created heavy quarks interactions. We calculate the background subtracted yield for the near side region $\Delta\phi \leq .942$, in the away side "head"

Associated p_T	$\Delta\phi$ region	Yield $\frac{1}{N_{trigger}\Delta\phi}$	Stat. Error	Sys. Error
$p_{T,asso} \in (.5, 1.0)$ GeV/c	Near-side	0.43422	0.152473	0.0568138
$p_{T,asso} \in (.5, 1.0)$ GeV/c	Head	0.868317	0.136648	0.0549569
$p_{T,asso} \in (.5, 1.0)$ GeV/c	Shoulder	0.37479	0.128162	0.00797441
$p_{T,asso} \in (1.0, 2.0)$ GeV/c	Near-side	0.39401	0.0845325	0.0303613
$p_{T,asso} \in (1.0, 2.0)$ GeV/c	Head	0.391791	0.0738275	0.0275223
$p_{T,asso} \in (1.0, 2.0)$ GeV/c	Shoulder	0.160784	0.0700681	0.0111099
$p_{T,asso} \in (2.0, 4.0)$ GeV/c	Near-side	0.0956762	0.0230099	0.00354069
$p_{T,asso} \in (2.0, 4.0)$ GeV/c	Head	0.107273	0.0231531	0.00321996
$p_{T,asso} \in (2.0, 4.0)$ GeV/c	Shoulder	0.0379724	0.0194678	0.00122931

Table 4.3: Yields and Errors from NPE-h correlations in 40-60% central Au+Au collisions with trigger 6.0GeV/c $\leq p_t \leq$ 9.0 GeV/c.

Associated p_T	$\Delta\phi$ region	Yield $\frac{1}{N_{trigger}\Delta\phi}$	Stat. Error	Sys. Error
$p_{T,asso} \in (.5, 1.0)$ GeV/c	Near-side	0.113593	0.0752799	0.0993901
$p_{T,asso} \in (.5, 1.0)$ GeV/c	Head	0.446483	0.0664356	0.0996666
$p_{T,asso} \in (.5, 1.0)$ GeV/c	Shoulder	0.351208	0.0655682	0.0254741
$p_{T,asso} \in (1.0, 2.0)$ GeV/c	Near-side	0.225576	0.0410495	0.0702893
$p_{T,asso} \in (1.0, 2.0)$ GeV/c	Head	0.234525	0.0363017	0.0692495
$p_{T,asso} \in (1.0, 2.0)$ GeV/c	Shoulder	0.0472435	0.035183	0.0101302
$p_{T,asso} \in (2.0, 4.0)$ GeV/c	Near-side	0.0771784	0.0115255	0.00835489
$p_{T,asso} \in (2.0, 4.0)$ GeV/c	Head	0.0855548	0.0104771	0.00824166
$p_{T,asso} \in (2.0, 4.0)$ GeV/c	Shoulder	0.0180967	0.00924105	0.0017841

Table 4.4: Yields and Errors from NPE-h correlations in 20-40% central Au+Au collisions with trigger 4.0GeV/c $\leq p_t \leq$ 6.0 GeV/c.

Associated p_T	$\Delta\phi$ region	Yield $\frac{1}{N_{trigger}\Delta\phi}$	Stat. Error	Sys. Error
$p_{T,asso} \in (.5, 1.0)$ GeV/c	Near-side	0.529239	0.16639	0.104476
$p_{T,asso} \in (.5, 1.0)$ GeV/c	Head	0.285343	0.147377	0.0922544
$p_{T,asso} \in (.5, 1.0)$ GeV/c	Shoulder	0.465791	0.144077	0.0391084
$p_{T,asso} \in (1.0, 2.0)$ GeV/c	Near-side	0.0457684	0.0909543	0.0497525
$p_{T,asso} \in (1.0, 2.0)$ GeV/c	Head	0.398024	0.0809105	0.0490142
$p_{T,asso} \in (1.0, 2.0)$ GeV/c	Shoulder	0.21068	0.0785307	0.0177771
$p_{T,asso} \in (2.0, 4.0)$ GeV/c	Near-side	0.183656	0.0245176	0.0100624
$p_{T,asso} \in (2.0, 4.0)$ GeV/c	Head	0.1675	0.0238689	0.00546355
$p_{T,asso} \in (2.0, 4.0)$ GeV/c	Shoulder	0.125145	0.0209576	0.00807931

Table 4.5: Yields and Errors from NPE-h correlations in 20-40% central Au+Au collisions with trigger 6.0GeV/c $\leq p_t \leq$ 9.0 GeV/c.

Associated p_T	$\Delta\phi$ region	Yield $\frac{1}{N_{trigger}\Delta\phi}$	Stat. Error	Sys. Error
$p_{T,asso} \in (.5, 1.0)$ GeV/c	Near-side	0.74085	0.167485	0.0727868
$p_{T,asso} \in (.5, 1.0)$ GeV/c	Head	0.737388	0.147269	0.0693534
$p_{T,asso} \in (.5, 1.0)$ GeV/c	Shoulder	0.658026	0.146362	0.0826822
$p_{T,asso} \in (1.0, 2.0)$ GeV/c	Near-side	0.223651	0.0911303	0.0636431
$p_{T,asso} \in (1.0, 2.0)$ GeV/c	Head	0.0738618	0.078665	0.0643826
$p_{T,asso} \in (1.0, 2.0)$ GeV/c	Shoulder	0.199047	0.0777526	0.0314492
$p_{T,asso} \in (2.0, 4.0)$ GeV/c	Near-side	0.0992778	0.0245557	0.0086265
$p_{T,asso} \in (2.0, 4.0)$ GeV/c	Head	0.0756338	0.0215144	0.00918282
$p_{T,asso} \in (2.0, 4.0)$ GeV/c	Shoulder	0.112994	0.0207828	0.0118356

Table 4.6: Yields and Errors from NPE-h correlations in 0-10% central Au+Au collisions with trigger 4.0GeV/c $\leq p_t \leq$ 6.0 GeV/c.

Associated p_T	$\Delta\phi$ region	Yield $\frac{1}{N_{trigger}\Delta\phi}$	Stat. Error	Sys. Error
$p_{T,asso} \in (.5, 1.0)$ GeV/c	Near-side	2.31516	0.358503	0.238676
$p_{T,asso} \in (.5, 1.0)$ GeV/c	Head	2.76404	0.316466	0.233436
$p_{T,asso} \in (.5, 1.0)$ GeV/c	Shoulder	2.84518	0.315039	0.180387
$p_{T,asso} \in (1.0, 2.0)$ GeV/c	Near-side	0.631058	0.193553	0.0816061
$p_{T,asso} \in (1.0, 2.0)$ GeV/c	Head	0.385498	0.172518	0.0558037
$p_{T,asso} \in (1.0, 2.0)$ GeV/c	Shoulder	0.283197	0.168621	0.0576901
$p_{T,asso} \in (2.0, 4.0)$ GeV/c	Near-side	0.326725	0.052348	0.0266922
$p_{T,asso} \in (2.0, 4.0)$ GeV/c	Head	0.151844	0.0469381	0.0147477
$p_{T,asso} \in (2.0, 4.0)$ GeV/c	Shoulder	0.134278	0.0464204	0.00730969

Table 4.7: Yields and Errors from NPE-h correlations in 0-10% central Au+Au collisions with trigger 6.0GeV/c $\leq p_t \leq$ 9.0 GeV/c.

$\Delta\phi \geq 2.2$, and in the away side shoulder $1.25 \leq \Delta\phi \leq 2.2$. For the separated shoulder and head regions we are looking for signs of away side broadening in the correlation. We might expect to find that the ratio of the shoulder to head yields is larger in more central collisions as a result of jets being diverted or smeared out as a result of interactions with the QGP. We can also look for evidence of medium responses to a heavy quark traversing it. The yields from these plots are listed in Table AAA. We will summarize these results once we have the correlations from p+p as well.

4.5 Correlations in p+p

With correlations from Au+Au collisions we can study the effects on observed particles resulting from heavy quark interactions with the medium. By looking across centralities we can select different fireball sizes and durations to see how the presence of QGP affects the formation of dijets. Now we can also look at p+p collisions also at $\sqrt{s_{NN}} = 200$ GeV to see the correlation without any QGP and use this as a baseline for comparison with our Au+Au results.

NPE-h correlations have also been used to study the charm to bottom produced in these collisions. This is done by fitting the observed correlations to Pythia simulations of NPE-h correlations from charm and bottom decays. Those resulting from bottom will have a broader distribution because of the higher mass of the B mesons compared to D. We will show a calculation of this as a consistency check with previous NPE-h analyses.

4.5.1 Data and Correlations

The dataset for the p+p correlations is the BHT triggered events in STAR run 12 p+p 200 GeV. The procedure for identifying non-photonic electrons and constructing the NPE-h correlation is nearly identical to Au+Au. We still need to perform the acceptance corrections as in Au+Au, however because of the lower multicplicities in p+p collisions it is difficult to get enough statistics for mixed event correlations so we will rely only on the single particle ϕ weighting. In run 12 the TPC perfomed much better and has a more uniform acceptance than in run 11 so practically these correction are far less important.

In p+p correlations there is no need to perform the background subtraction as in Equation 4.1 since there is no elliptic flow in p+p collisions. So we no longer need to consider raw correlations, we can just take the results from Equation 4.2 and use those as our correlations. Since there is no NPE-h v_2 and no need to normalize to some background distribution we no longer have to consider 2 of the 3 sources of systematic uncertainty present in Au+Au. We only need to account for uncertainty in ϵ_γ, the photonic electron reconstruction efficiency. We do this as in Au+Au collisions, allowing the efficiency to vary by 10%. Tables 4.8 4.9 summarize the yields with errors obtained from p+p collisions.

4.5.2 Charm to Bottom Ratios

We can use the p+p NPE-h correlations to investigate the relative contributions of charm and bottom to non-photonic electrons by fitting the observed correlations with those from B and D to find the ratio as a function of electron p_T. Several experiments have performed this measurement, making this a reasonable check that our method for constructing NPE-h

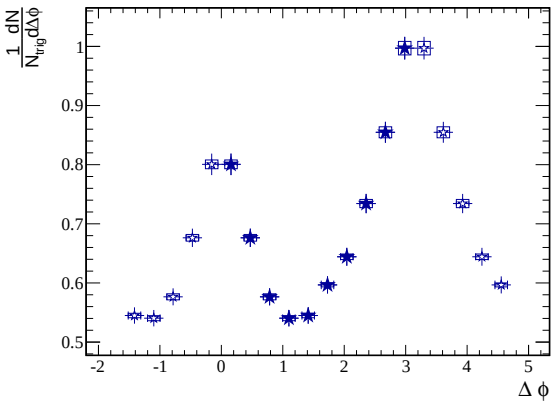

(a) .5 GeV/c $\leq p_{T,h} \leq$ 1.0 GeV/c

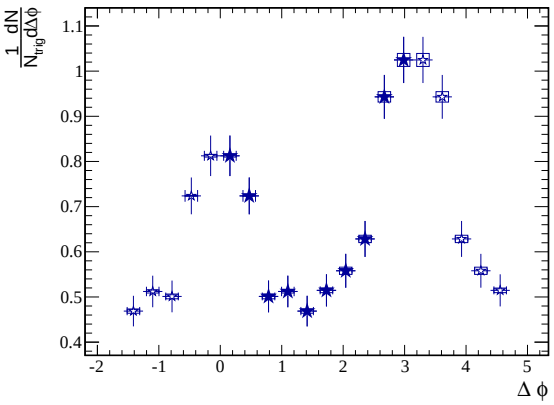

(b) .5 GeV/c $\leq p_{T,h} \leq$ 1.0 GeV/c

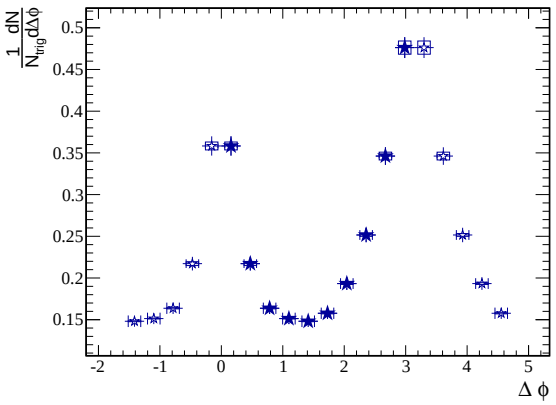

(c) 1.0 GeV/c $\leq p_{T,h} \leq$ 2.0 GeV/c

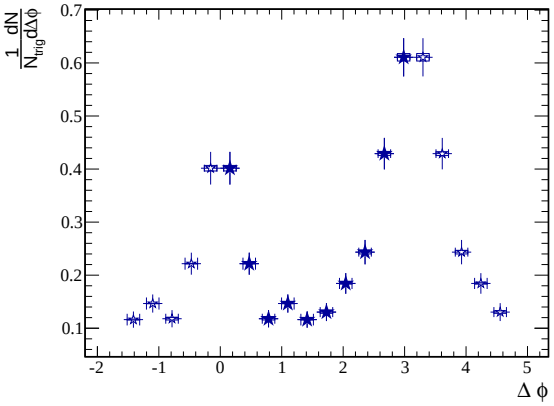

(d) 1.0 GeV/c $\leq p_{T,h} \leq$ 2.0 GeV/c

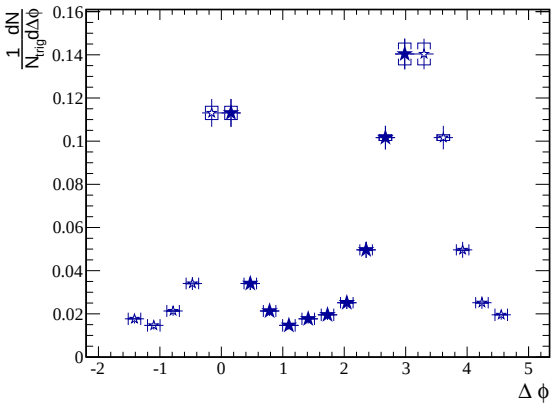

(e) 2.0 GeV/c $\leq p_{T,h} \leq$ 4.0 GeV/c

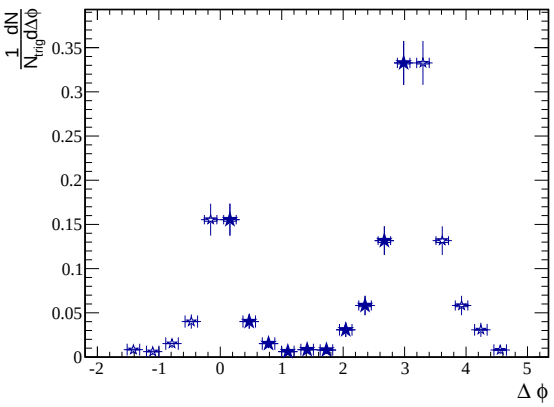

(f) 2.0 GeV/c $\leq p_{T,h} \leq$ 4.0 GeV/c

Figure 4.12: NPE-h correlations for p+p collisions at 200 GeV left column shows triggers with 4.0Gev/c$\leq p_T \leq$ 6.0 GeV/c and right column is 6.0Gev/c$\leq p_T \leq$ 9.0 GeV/c.

Associated p_T	$\Delta\phi$ region	Yield $\frac{1}{N_t rigger \Delta\phi}$	Stat. Error	Sys. Error
$p_{T,asso} \in (.5, 1.0)$ GeV/c	Near-side	0.814888	0.00977926	0.00360017
$p_{T,asso} \in (.5, 1.0)$ GeV/c	Head	0.812439	0.00965688	0.00511522
$p_{T,asso} \in (.5, 1.0)$ GeV/c	Shoulder	0.561056	0.00786714	0.00216749
$p_{T,asso} \in (1.0, 2.0)$ GeV/c	Near-side	0.279777	0.00536135	0.00167489
$p_{T,asso} \in (1.0, 2.0)$ GeV/c	Head	0.337404	0.00580794	0.00293765
$p_{T,asso} \in (1.0, 2.0)$ GeV/c	Shoulder	0.156817	0.00379766	0.000439399
$p_{T,asso} \in (2.0, 4.0)$ GeV/c	Near-side	0.057533	0.00242196	0.00096921
$p_{T,asso} \in (2.0, 4.0)$ GeV/c	Head	0.0916335	0.0030426	0.00164648
$p_{T,asso} \in (2.0, 4.0)$ GeV/c	Shoulder	0.019603	0.00132994	8.75715e-05

Table 4.8: Yields and Errors from NPE-h correlations in p+p collisions with trigger 4.0GeV/c $\leq p_t \leq$ 6.0 GeV/c.

Associated p_T	$\Delta\phi$ region	Yield $\frac{1}{N_t rigger \Delta\phi}$	Stat. Error	Sys. Error
$p_{T,asso} \in (.5, 1.0)$ GeV/c	Near-side	0.801004	0.0245826	0.00217934
$p_{T,asso} \in (.5, 1.0)$ GeV/c	Head	0.815639	0.025429	0.00632914
$p_{T,asso} \in (.5, 1.0)$ GeV/c	Shoulder	0.48424	0.0194036	0.00332109
$p_{T,asso} \in (1.0, 2.0)$ GeV/c	Near-side	0.278887	0.0138082	0.00181987
$p_{T,asso} \in (1.0, 2.0)$ GeV/c	Head	0.403106	0.0163408	0.00270691
$p_{T,asso} \in (1.0, 2.0)$ GeV/c	Shoulder	0.135421	0.00940179	0.000890293
$p_{T,asso} \in (2.0, 4.0)$ GeV/c	Near-side	0.0681146	0.00652803	0.000581799
$p_{T,asso} \in (2.0, 4.0)$ GeV/c	Head	0.164206	0.00992462	0.000868219
$p_{T,asso} \in (2.0, 4.0)$ GeV/c	Shoulder	0.0147791	0.00321696	0.000280081

Table 4.9: Yields and Errors from NPE-h correlations in p+p collisions with trigger 6.0GeV/c $\leq p_t \leq$ 9.0 GeV/c.

correlations is working as intended.

The simulations are done with Pythia 8.2 with the standard STAR heavy flavor tune. To get reasonable samples across all electron p_T and to avoid the low p_T divergence in heavy flavor processes in Pythia we generate the correlations in several bins in `ptHat` and then piece them together according to a weighting, this closely follows the Pythia example `main08.cc`. For `ptHat` ≤ 3.0 GeV/c we use the "minbias" process `SoftQCD:nonDiffractive = on` for the bins above this we use the hard QCD processes `HardQCD:all = on`. Then to patch the different bins together we scale each bin by the generated cross section, the raw and scaled `ptHat` spectra can be seen in Figure 4.13.

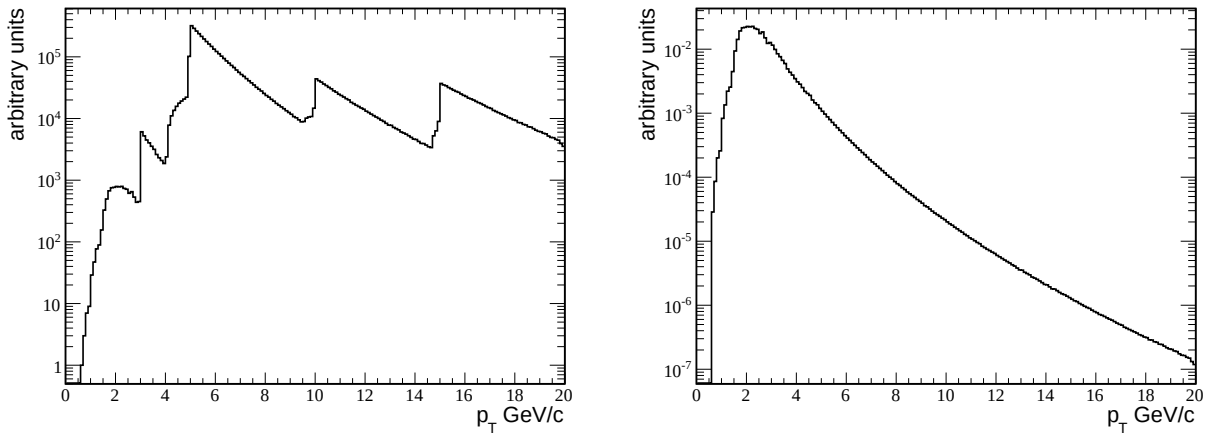

(a) Raw

(b) Weighted

Figure 4.13: The raw and weighted `ptHat` spectra from Pythia.

Then we construct the electron-hadron correlations from the Pythia simulations in two separate cases one for initial b quarks and one for initial c quarks. We check that the final state contains an electron and that the electron has a parent B or D meson. To increase statistics, if there is no final state electron we we pick on of the heavy mesons, undo and then redo the decay until we get an electron effectively setting the branching ratio for semileptonic decays to 100%. Then we apply acceptance cuts that closely match the STAR acceptance: $\eta_e \in (-.7, .7)$, $p_{T,e} > 2.0$ GeV/c,$\eta_h \in (1.0, 1.0)$, and $p_{T,h} > 0.2$ GeV/c. This gives us the electron-hadron correlation that we use in the fit.

For the fit we compare the correlations for $p_{T,h} > .2$ GeV/c and vary the p_T of the trigger particle. We fit the correlation with the function:

$$\frac{dN_{NPE-h}}{d\Delta\phi} = r_B f_B(\Delta\phi) + (1 - r_B) f_D(\Delta\phi) \tag{4.3}$$

Where f_B and f_D are the correlations for bottom and charm electron-hadron correlations from Pythia, and $r_B = \frac{e_B}{e_B + e_D}$. The fit is done in a range around the near side peak $\Delta\phi < 1.5$ due to diffuculties in Pythia accurately recreating away side behavior. Figure 4.14 shows an example fit, plus the correlations from Pythia.

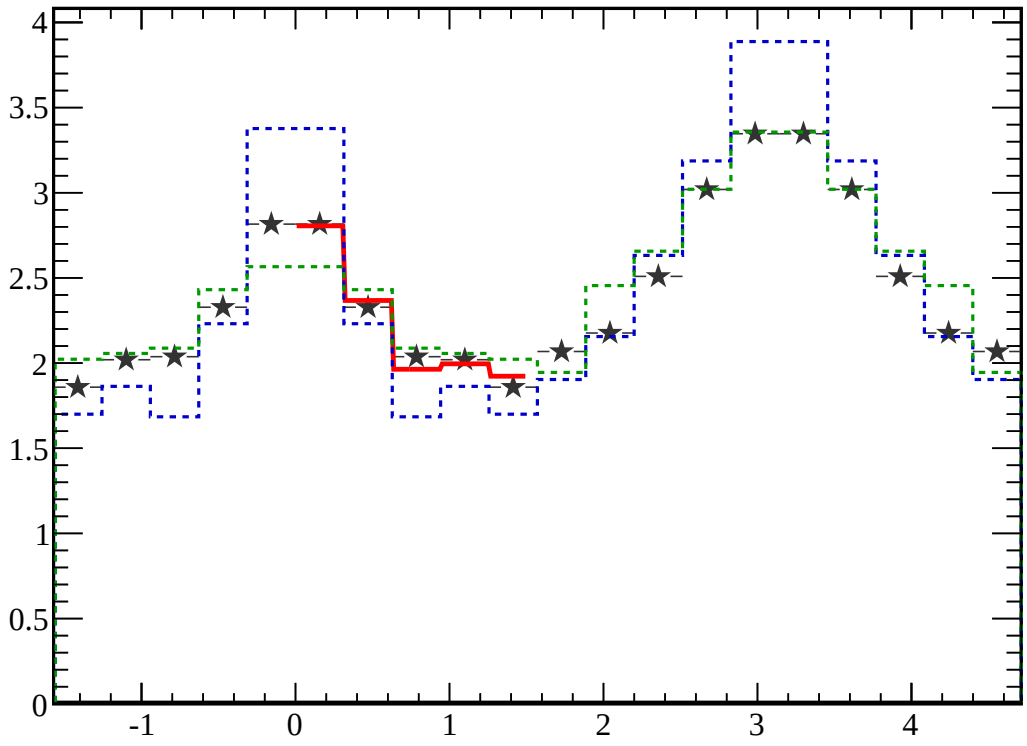

Figure 4.14: NPE-h correlation with 5.0 GeV/c $< p_{T,e} <$ 6.0 GeV/c and $p_{T,h} > 0.2$ GeV/c. Pythia distributions are $f_D(\Delta\phi)$ (blue), $f_B(\Delta\phi)$ (green), and the distribution with best fit value of r_B (red).

Figure 4.15 shows the results for obtaining r_B from fits of the p+p correlation plus

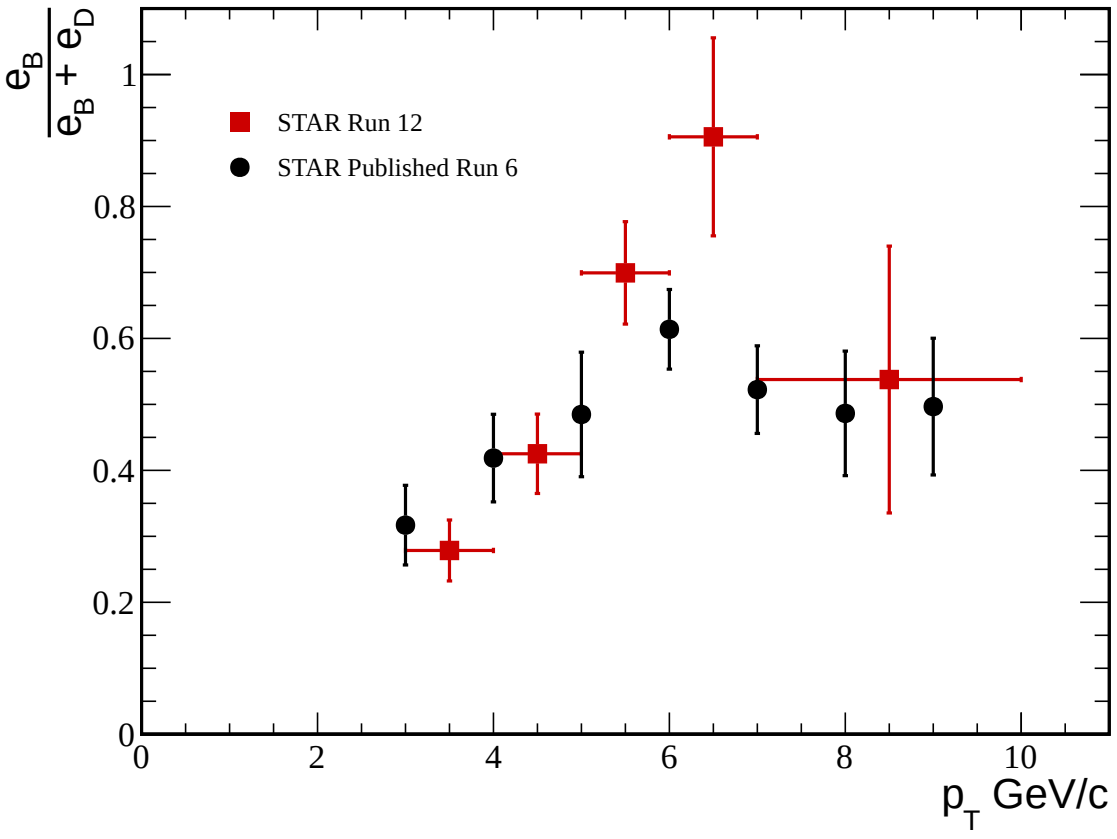

Figure 4.15: Measured value of r_B as a function of trigger p_T. Red points are for the current analysis and the black are from STAR published in Ref. Only statistical errors are shown.

a comparison to previous published results. Errors are large at high trigger p_T due to the distributions from B and D becoming similar thus reducing the ability to distinguish between the contributions to the overall p+p correlation shape. Discrepancies in the mid p_T range may be due to difficulties in patching together the `ptHat` bins in the Pythia simulations and this could be fixed by only using `SoftQCD:nonDiffractive` to generate the simulated correlations, but this would be far more time consuming.

4.6 Comparisons of Yields

We can use the yields we measured in p+p and Au+Au collisions to look for evidence of jet modification in the medium. To do this we will examine the away side peak shape by comparing the ratio of yields in the shoulder region to the head region (as defined previously). Interactions with the QGP may cause jets to be redirected or smeared out which would manifest as broader away side correlatins in Au+Au collisions. We will also look at I_{AA}, the ratio of the integrated yield in Au+Au to p+p. Suppressions of yields in Au+Au could indicate jet suprression in the medium while increased yields may point to medium responses to the jet.

An important thing to note when comparing the yields from p+p and Au+Au is that we subtracted off a background correlation from Au+Au but performed no such ZYAM procedure for p+p. There is no standard way of accounting for this but we calculate a flat underlying event for p+p (essentially the ZYAM coefficient for background with $v_2 = 0$), use this to estimate the oversubtraction of background in Au+Au and add this back to the Au+Au yields. As seen in Figure 4.12, this is not much of a concern at high associated hadron p_T but for the lower p_T bins it has a larger effect.

4.6.1 Away Side Shape

We define the yield Y in a region by:

$$Y(\Delta\phi_1, \Delta\phi_2) = \int_{\Delta\phi_1}^{\Delta\phi_2} \frac{dN_{NPE-h}}{d\Delta\phi} d\Delta\phi \tag{4.4}$$

We define the near side yield as $Y(0, 2\pi/5)$ the head region as $Y(7\pi/10, \pi)$, and the shoulder region as $Y(2\pi/5, 7\pi/10)$. To see evidence of jet broadening we compare the yields in the shoulder and head regions. In particular we look at the ratio of the yields $Y(\text{shoulder})/Y(\text{head})$. We can see from the p+p data that this ratio tends to be below 1 as the away side peaks are narrow and contain most of the yield in the region immediately around π. Figure 4.16 shows the the ratios for p+p data as well as Au+Au collisions with 0-10%, 10-40%, and 40-60% centralities. We see that for the most central bins the ratio is larger indicating wider correlations, but the errors on these yields are large. For the other bins, including the p+p data, the ratios seem to follow a similar trend with increasingly narrow correlations at higher hadron p_T.

4.6.2 I_{AA}

We can also compare the yields in Au+Au collisions to p+p collisions directly to look for jet supression in heavy flavor correlations. To do this we look at the ration of yields I_{AA} defined by:

$$I_{AA} = \frac{Y_{AuAu}(\Delta\phi_1, \Delta\phi_2)}{Y_{pp}(\Delta\phi_1, \Delta\phi_2)} \tag{4.5}$$

I_{AA} serves for jets as a rough analogue of R_{AA} which is typically used to compare particle spectra between heavy-ion and proton collisions. For identical yields in Au+Au and p+p we would get $I_{AA} = 1$ and we look for deviations from 1, less than 1 indicating suppressed yield in Au+Au and greater than 1 an enhanced yield.

We measure I_{AA} for the near side as well as in the away side head region. As explained earlier we estimate the level for the underlying event in p+p and then add this back to the Au+Au data to make up for potential oversubtraction of background with the ZYAM normalization. Figure 4.17 show the near side I_{AA} and Figure 4.18 the away side. The results are largely inconclusive and it appears that with the errors the results are still largely consistent with 1.

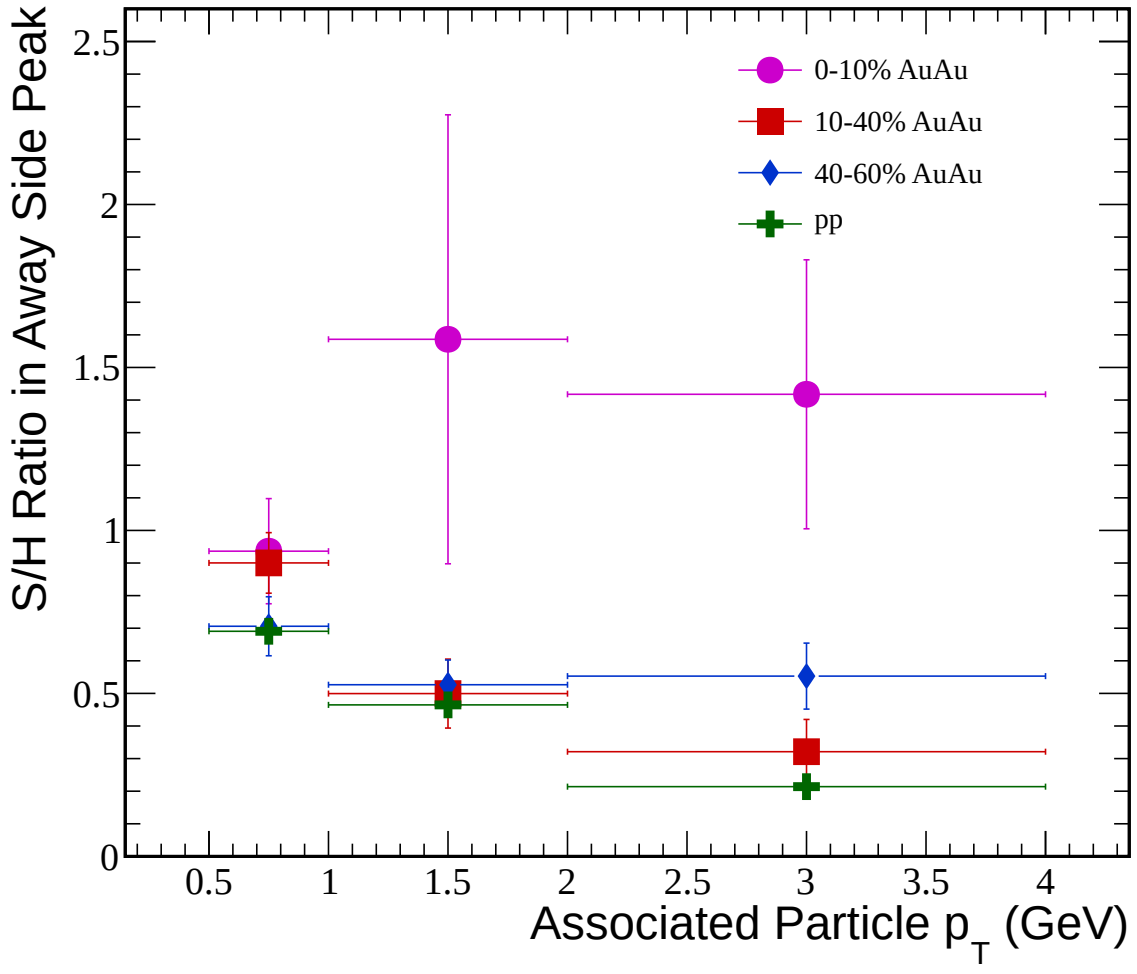

Figure 4.16: Ratio of yields in shoulder region to head region in NPE-h correlations for trigger electrons have 4.0 GeV/c $\leq p_T \leq$ 6.0 GeV/c. A larger ratio indicates a wider peak.

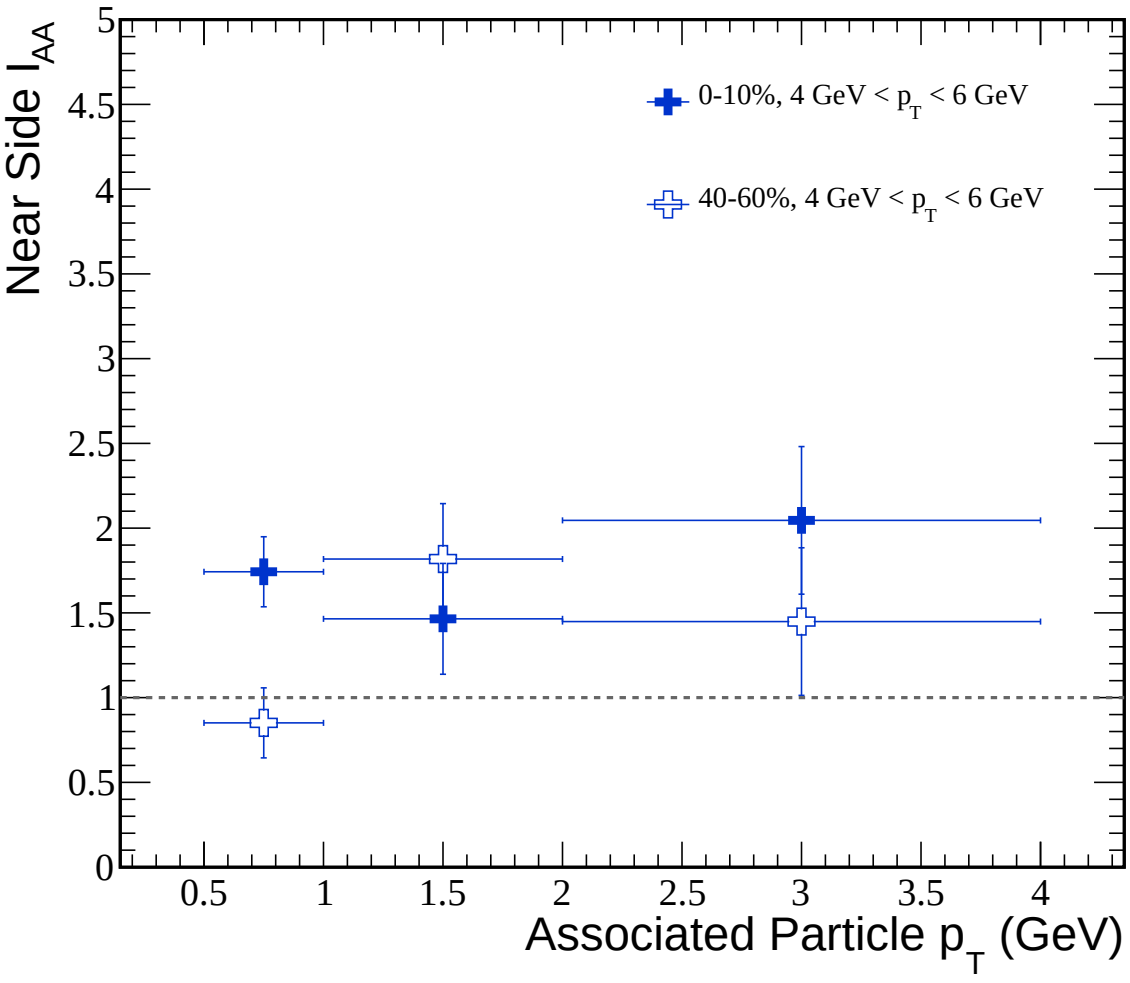

Figure 4.17: Near side

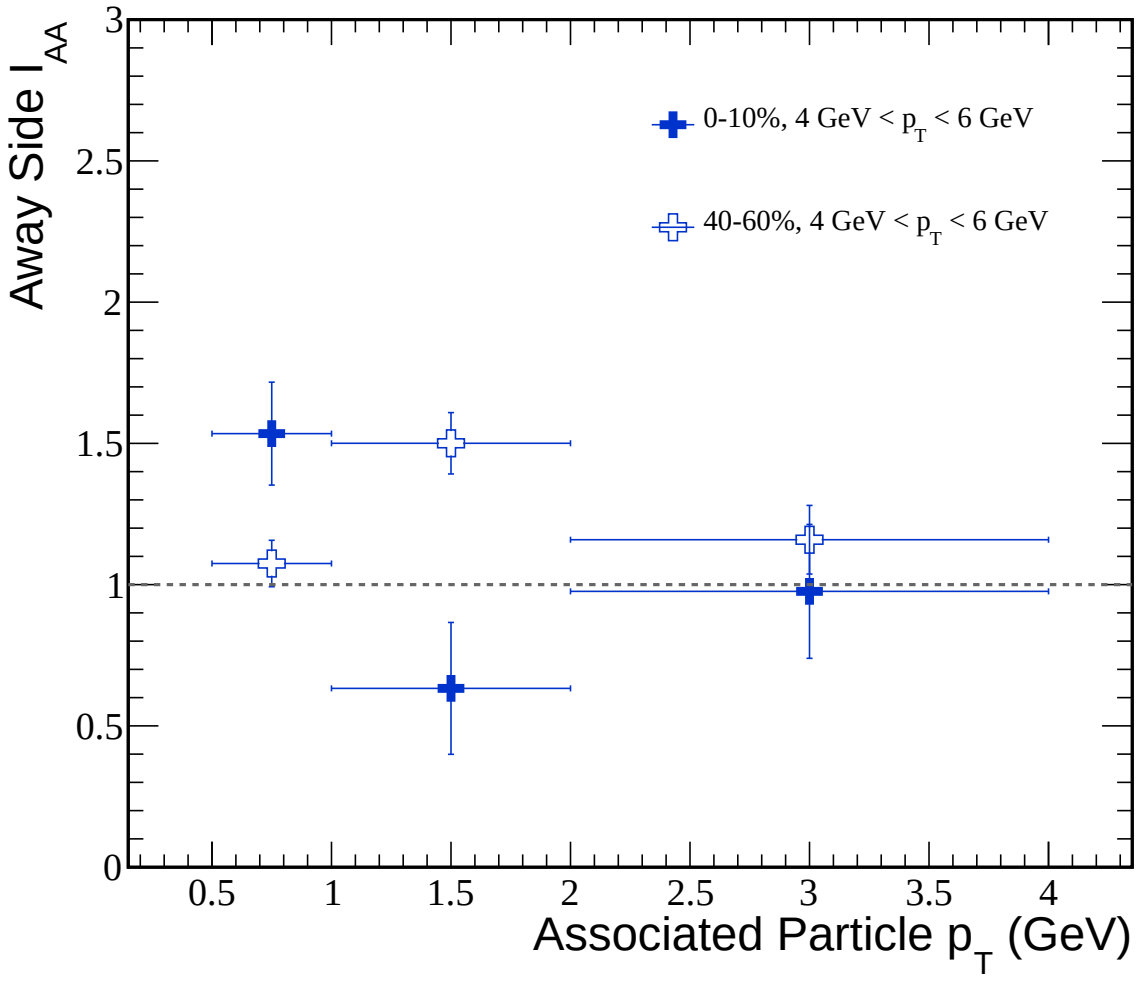

Figure 4.18: Away side

4.7 Event-Plane Dependent Correlations

The motivation for measurements of two particle correlations in Au+Au comes from the fact that partons are expected to strongly interact with the color charges present in QGP and that the jet like correlations will depend on the path length traversed by the parton in QGP. Previously we have looked at comparisons between central and peripheral events as well as p+p collisions as a way of investigating the dependnce on the presence of QGP. Now we will try to look at a more direct dependence on path length by measuring the correlations relative to emmision in or out of the event plane.

In non-central Au+Au collisions the collision region formed from the overlap of the two incident nuclei is ellipsoidal. This initial anisotropy in the medium results in elliptic flow, v_2, and in the final state we observe anisotropic emissions relative to the reaction plane, defined by the momenta of the initial beam particles (see Figure 4.19).

Elliptic flow is defined relative to the reaction plane, however there is no way to experimentally determine the reaction plane in a given event. Instead we use the azimuthal distribution of observed particle to estimate the reaction plane. We get an angle for the estimated reaction plane which we call the event plane. Due to the fact that we calculate the event plane from a finite number of particles we also have some resolution of our event plane angle.

The event plane angle gives us an estimate for the reaction plane angle, we will then look at our trigger particle's angle relative to the event plane. As seen in Figure 4.19 particles traversing the medium perpendicular to the event plane should move through a larger part of the medium. We might guess that out-of-plane correlations show larger away side suppression compared to in-plane, which has already been observed in dihadron correlations. A large portion of our high tower trigger data comes from mid-centralities (30-60% central) which is useful for this analysis since that is where we have the best event plane resolution, but due to higher hadron v_2 this region also has larger systematic uncertainties which may make drawing conclusions difficult.

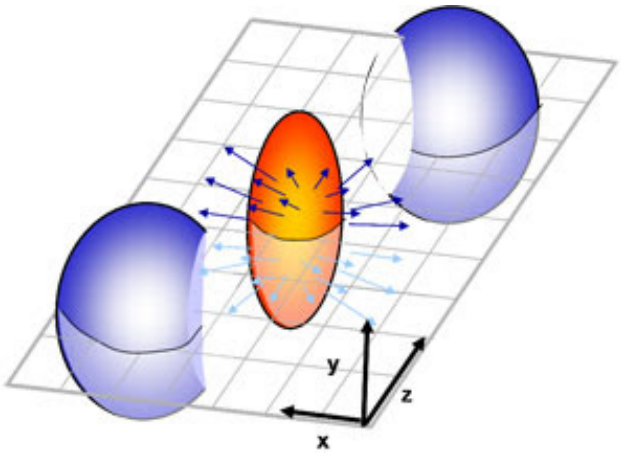

Figure 4.19: Illustration of non-central heavy ion collision and the resulting v_2. The reaction plane corresponds to the xz-plane in the diagram.

4.7.1 Event Plane Reconstruction

We use the azimuthal distribution of the particles in an event to calculate the event plane, Ψ_{EP}. Event planes can be calculated for any order of harmonic in the decompisition of the particle distribution, but since we are interested in v_2 and the second order event plane everything that follows is specifically the $n = 2$ case. For a more general treatment see ref. First we apply single particle ϕ-weighting to correct for the acceptance of the detector. This is the same procedure as used for the two-particle correlation.

We use the hadrons in the event with 0.2 GeV/c $\leq p_T \leq$ 2.0 GeV/c in the event plane calculation. Since these events are high tower triggered events there is also a high p_T leading particle in each event. Since the presence of a jet may bias the calculation of the event plane, we should try to remove this contribution. To do this we exclude the particles in the event with $|\Delta\eta| < .5$, where $\Delta\eta$ is the pseudorapidity difference between the hadron and the leading particle in the event (in events used in NPE analysis this track is usually the electron). This procedure is called the Modified Reaction Plane (MRP) method.

With our sample of hadrons we then construct a flow vector $\mathbf{Q}$ for the event. The components of this vector are:

$$X = \sum_i w_i \cos(2\phi_i) \tag{4.6}$$

$$Y = \sum_i w_i \sin(2\phi_i) \tag{4.7}$$

where w_i is some weight given to the particle, in this analysis we use the particle's p_T as the weight. The second order event plane angle is then given by:

$$\Psi_{EP} = \frac{1}{2}\tan^{-1}(\frac{Y}{X}) \tag{4.8}$$

The true distribution of the reaction planes should be uniform across all events, however there will still be some distortion in the event plane distribution which we need to correct. To do this we use a shifting method where the harmonics of the uncorrected distribution are used to flatten it. Figure 4.20 shows the distribution of the event plane angle after applying the shifting correction. We see that the resulting distribution is flat to within 1%.

When we calculate the event plane dependent NPE-h correlations we will potentially be correlating the trigger electron with some of the particles used in the event plane calculation. We would like the calculated event plane to be independent of the particles in the correlation so we will actually calculate 5 separate event planes per event. We calculate one for all hadrons in the range .2 GeV/c $\leq p_T \leq$ 2.0 GeV/c then we calculate one for each case where the ranges .2 GeV/c $\leq p_T \leq$ .5 GeV/c, .5 GeV/c $\leq p_T \leq$ 1.0 GeV/c, 1.0 GeV/c $\leq p_T \leq$ 1.5 GeV/c, and 1.5 GeV/c $\leq p_T \leq$ 2.0 GeV/c are excluded. Each bin with an excluded p_T range will have a lower resolution due to fewer particles used in the event plane calculation.

Using a finite number of particles to calculate the event plane leaves us with an event plane resolution by which we must scale up our azimuthal anisotropy measurements to get the anisotropy relative to the true reaction plane. This is done to get the correct value of v_2 in flow analyses but we will also need the event plane resolution for calculating the event plane dependent v_2 background for electron-hadron correlations. We calculate the resolution by subevent planes. We divide each event randomly into two equally sized sub events then independently calculate the event plane for each. The differences between the subevent

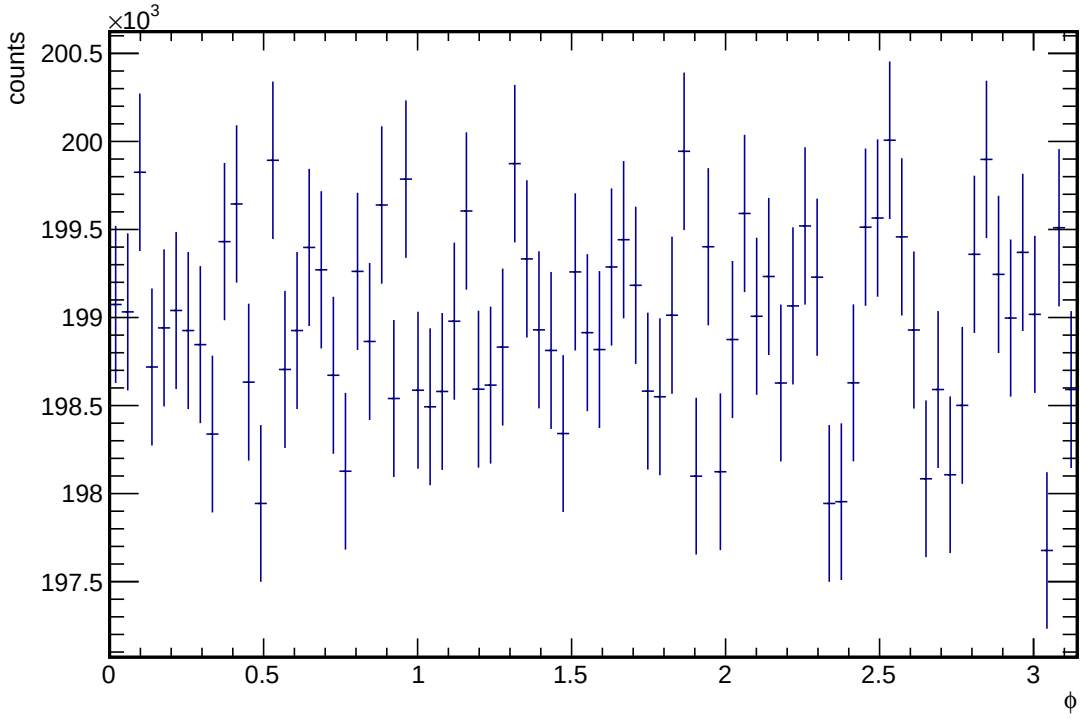

Figure 4.20: The ϕ distribution of the event plane angle Ψ_{EP} after applying the shifting correction.

planes can be used to measure the event plane resolution. Figure 4.21 summarizes the resolution as a function of event centrality as well for different hadron p_T slices. Resolution is best around 30% centrality and falls off in central events due to lower azimuthal anisotropy and in peripheral events because of lower multiplicity.

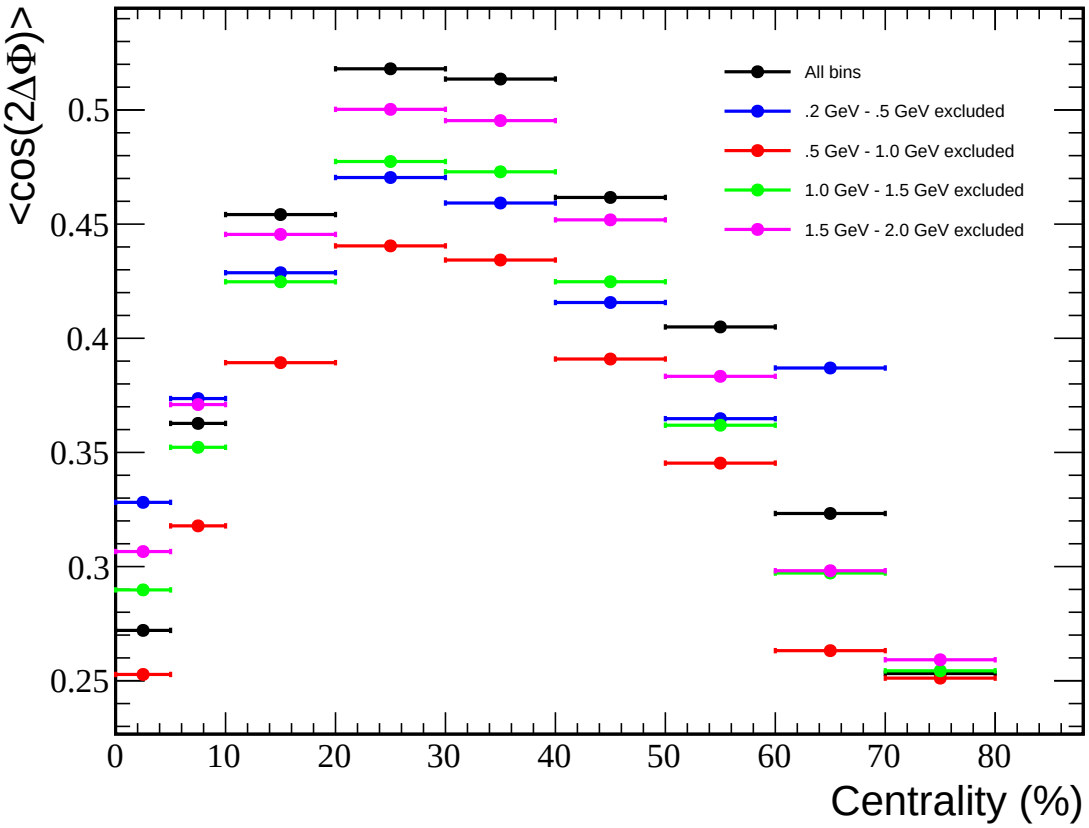

Figure 4.21: Event plane resolution as a function of centrality.

4.7.2 Correlations

Now we would like to calculate the NPE-h correlation and look at the dependence based on how the trigger particle is oriented relative to the event plane. Since for trigger particles which are out of the event plane the heavy quark traversed a longer path in medium, we might wonder if this could effect the correlation.

The correlation is constructed as previously described for Au+Au collisions with one important difference. Before the background from flow assumed no dependence of the trigger particle on the reaction plane. The form of this background resulted from the dependence on the reaction plane cancelling leaving only the difference $\Delta\phi$ between the correlated particles. Now we are choosing specific orientations of the trigger particle relative to the event plane and thus the background will be different and depend on that orientation.

We use the same functional form for the background, Equation 4.1, as when we originally calculated the NPE-h correlations in Au+Au, but now we replace the v_2 of the electron with an 'effective' v_2, denoted $\widetilde{v}_2$, which will depend on the electrons angle relative to the event plane as well as the event plane resolution. The effective v_2 can be calculated for any arbitrary slice relative to the event plane, but we will only consider the case of two equal slices: in-plane and out-of-plane. For this case $\widetilde{v}_2$ is given by:

$$0 \leq |\phi_{trig} - \Psi_{EP}| \leq \frac{\pi}{4} : \widetilde{v}_2 = \frac{\pi v_2 + 2\langle\cos(2\Delta\Psi)\rangle}{\pi + 4v_2\langle\cos(2\Delta\Psi)\rangle} \tag{4.9}$$

$$\frac{\pi}{4} \leq |\phi_{trig} - \Psi_{EP}| \leq \frac{\pi}{2} : \widetilde{v}_2 = \frac{\pi v_2 - 2\langle\cos(2\Delta\Psi)\rangle}{\pi - 4v_2\langle\cos(2\Delta\Psi)\rangle} \tag{4.10}$$

where Equation 4.9 is for in-plane triggers and Equation 4.10 is for out-of-plane triggers.

Now we construct the raw correlations for two cases: The trigger particle is in-plane or out-of-plane and then subtract off the appropriate background for that case. We use the ZYAM method to normalize the bckground to the distributions, calculating each case individually. In principle it is possible to calculate what the normalization for each case should be just from the normalization of the background for all triggers, but we choose not to do this. When combining bins in centrality we calculate $\widetilde{v}_2$ from the average values in each bin, weighted by the number of NPE in each centrality bin.

We construct the raw correlation for 20-60% central events. This is the region with the best event plane resolution due to the large elliptic flow and high multiplicity. It is also similar to the centrality region investigated by previous analyses of event plane dependent dihadron correlations. Figure 4.22 shows the resulting raw correlations for both cases and

the dependence on the associated hadron p_T. We can also see how the background changes between in-plane and out-of-plane cases. For out-of-plane triggers the background appears shifted by $\pi/2$ since the effective v_2 has a negative value. This is not always the case though as for bins with large v_2 but poor event plane resolution we could potentially find that $\widetilde{v}_2$ for out-of-plane triggers is still positive.

We can then subtract the backgrounds to get the correlations and yields to see if there is any significant difference between the in-plane and out-of-plane cases. The systematic errors from photonic eletron reconstruction efficiency and background normalization are calculated exactly as before. For the uncertainty in NPE v_2 we again let the value vary between .05 and .15 calculate $\widetilde{v}_2$ for the extreme values and then take the difference between the points when fit with different backgrounds as the uncertainty.

We can see from the subtracted distributions in Figure 4.23 that systematic uncertainties are quite large for lower hadron p_T. Above 2 GeV/c the uncertainties are less of a problem and this also happens to be the exact region looked at by a previous STAR analysis in dihadron collisions. In Figure 4.24 we show the comparison of in-plane and out-of-plane correlations for NPE-h as well as dihadron correlations, p+p dihadron correlations are also shown. For the dihadron correlations only the statistical errors are shown. We see that while in dihadron correlations there is evidence of greater jet supression in the out-of-plane correlations, there does not appear to be any discernable difference between in-plane and out-of-plane in NPE-h correlations. In fact, the NPE-h correlations appear comparable to the dihadron p+p data. There are a few possible explanations for this. The NPE-h correlation contains the decay products of the heavy B or D meson which happens after the freezeout of the QGP. Also in heavy flavor correlations the connection of the kinematics of the leading particle to the initial heavy quark is more tenuous, and the biases in these correlations may be different. We won't draw any definitive conclusions from these data and instead just present them as potential avenues for further study.

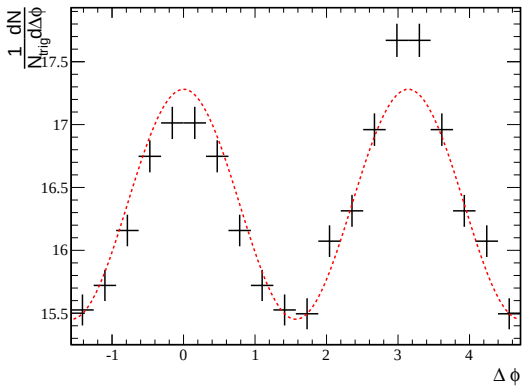

(a) .5 GeV/c $\leq p_{T,h} \leq$ 1.0 GeV/c

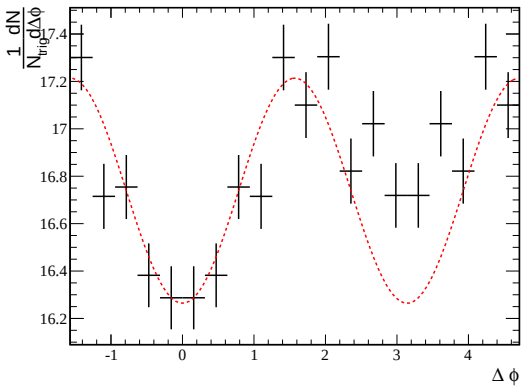

(b) .5 GeV/c $\leq p_{T,h} \leq$ 1.0 GeV/c

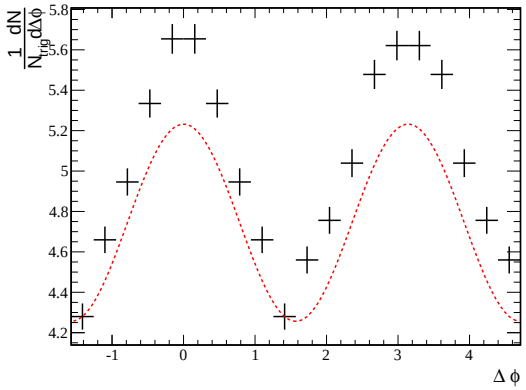

(c) 1.0 GeV/c $\leq p_{T,h} \leq$ 2.0 GeV/c

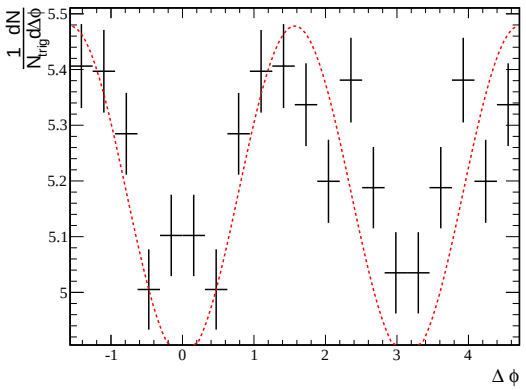

(d) 1.0 GeV/c $\leq p_{T,h} \leq$ 2.0 GeV/c

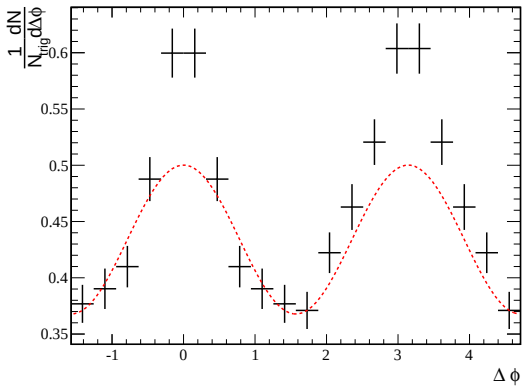

(e) 2.0 GeV/c $\leq p_{T,h} \leq$ 4.0 GeV/c

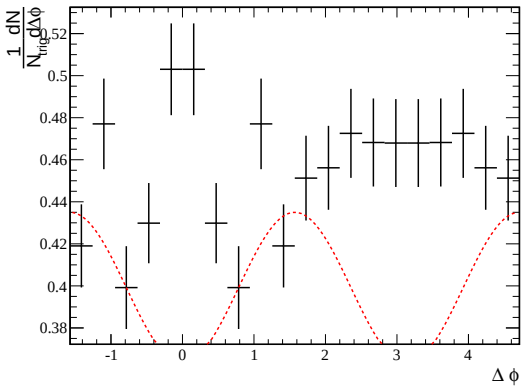

(f) 2.0 GeV/c $\leq p_{T,h} \leq$ 4.0 GeV/c

Figure 4.22: Raw NPE-h correlations for 20-60% centrality Au+Au collisions with 4.0 GeV/c $\leq pt_{T,e} \leq$ 6.0 GeV/c. Left column shows correlations for in-plane electrons, right shows out-of-plane electrons.

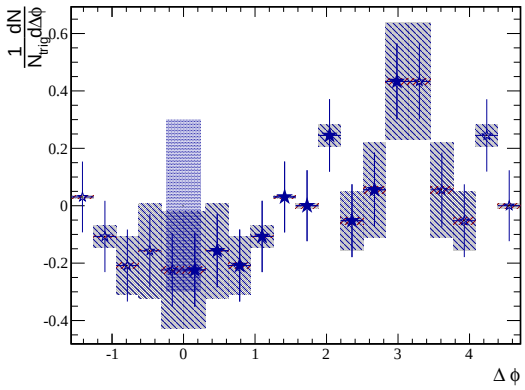

(a) .5 GeV/c $\leq p_{T,h} \leq$ 1.0 GeV/c

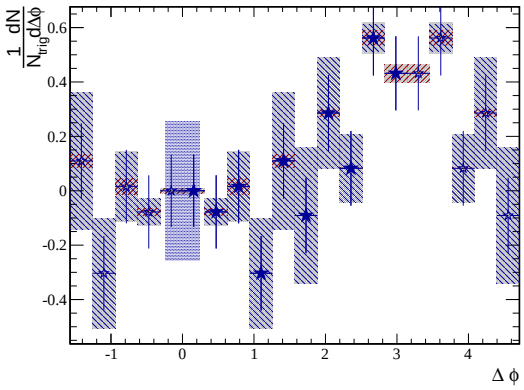

(b) .5 GeV/c $\leq p_{T,h} \leq$ 1.0 GeV/c

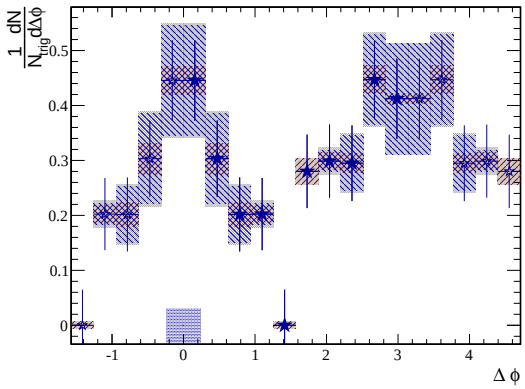

(c) 1.0 GeV/c $\leq p_{T,h} \leq$ 2.0 GeV/c

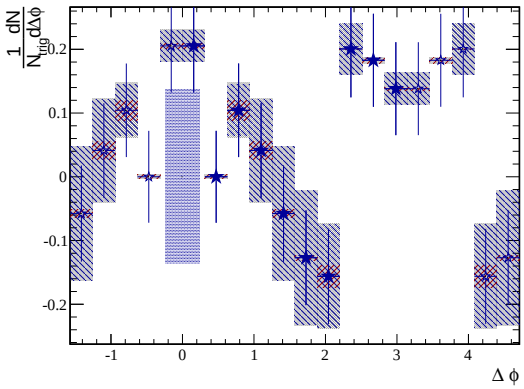

(d) 1.0 GeV/c $\leq p_{T,h} \leq$ 2.0 GeV/c

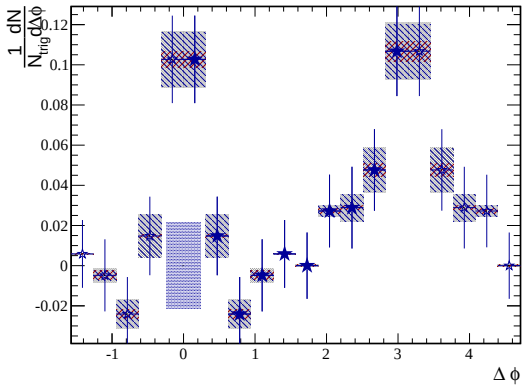

(e) 2.0 GeV/c $\leq p_{T,h} \leq$ 4.0 GeV/c

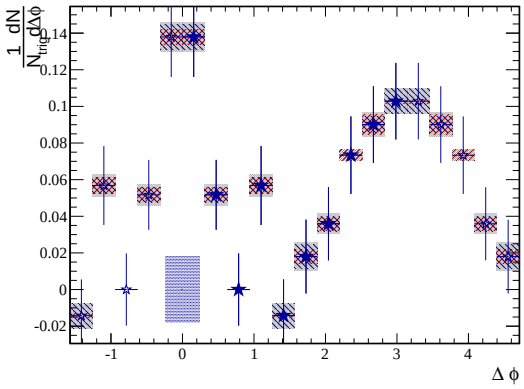

(f) 2.0 GeV/c $\leq p_{T,h} \leq$ 4.0 GeV/c

Figure 4.23: NPE-h correlations for 20-60% centrality Au+Au collisions with 4.0 GeV/c $\leq pt_{T,e} \leq$ 6.0 GeV/c. Left column shows correlations for in-plane electrons, right shows out-of-plane electrons. Errors from photonic eletron reconstruciton efficiency and NPE v_2 uncertainty are shown as shaded regions around each point, background normalization uncertainties are the shaded bars around 0.

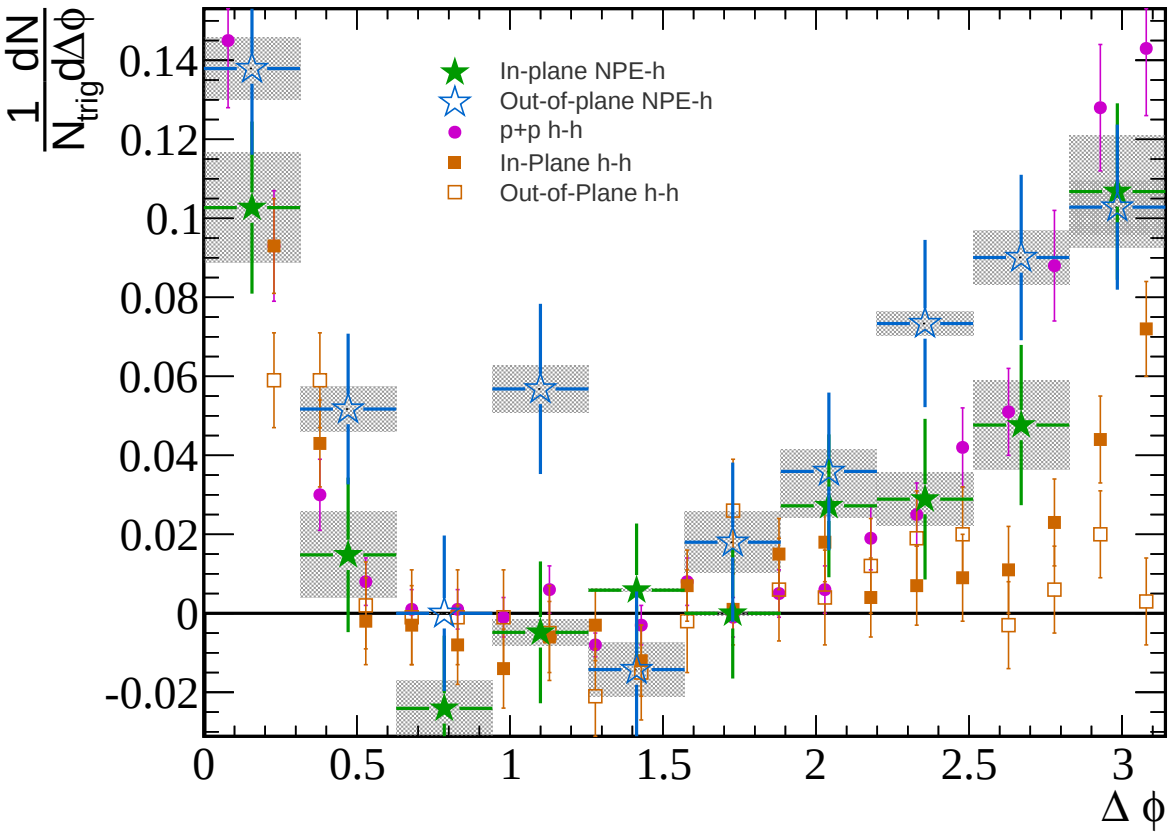

Figure 4.24: In-plane and out-of-plane correlations comparison for NPE-h and dihadron correlations.